Universidade do Minho
Escola de Medicina

Sofia Libório Passos Ramos

Macrophages in pulmonary fibrosis: characterization and fibroblasts transdifferentiation modulation

outubro de 2019

Sofia Libório Passos Ramos **Macrophages in pulmonary fibrosis: characterization and fibroblasts transdifferentiation modulation**

UMinho|2019

Universidade do Minho
Escola de Medicina

Sofia Libório Passos Ramos

Macrophages in pulmonary fibrosis: characterization and fibroblasts transdifferentiation modulation

Dissertação de Mestrado
Mestrado em Ciências da Saúde

Trabalho efetuado sob a orientação da
Doutora Sandra Maria Araújo da Costa

outubro de 2019

DIREITOS DE AUTOR E CONDIÇÕES DE UTILIZAÇÃO DO TRABALHO POR TERCEIROS

Este é um trabalho académico que pode ser utilizado por terceiros desde que respeitadas as regras e boas práticas internacionalmente aceites, no que concerne aos direitos de autor e direitos conexos.

Assim, o presente trabalho pode ser utilizado nos termos previstos na licença abaixo indicada.

Caso o utilizador necessite de permissão para poder fazer um uso do trabalho em condições não previstas no licenciamento indicado, deverá contactar o autor, através do RepositóriUM da Universidade do Minho.

Licença concedida aos utilizadores deste trabalho



Atribuição-NãoComercial-SemDerivações
CC BY-NC-ND

https://creativecommons.org/licenses/by-nc-nd/4.0/

Agradecimentos

Primeiramente gostaria de agradecer à minha orientadora, Sandra Costa, pela paciência, apoio, oportunidades e ensinamentos. Já são uns anos a aturar-me, sei que não é fácil, mas até que é divertido.

Às minhas companheiras e amigas, Caroline e Catarina, palavras nunca chegarão para vos agradecer todo o apoio, por as todas as horas, pela felicidade que me dava ir trabalhar ao vosso lado! Se cheguei ao fim foi muito graças a vocês! A elas junto a nossa Cris, muito obrigada pelos momentos de descontração! Levar-vos-ei para a vida meninas!

À Marta, Bruna, Joana, Catarina, Andreia e Nuno, que grupo maravilha que aqui se formou! Obrigada principalmente por me fazerem rir sempre e por todo o apoio!

À Bárbara, obrigada por me ensinares e apoiares quer a nível profissional quer a nível pessoal! És um exemplo e és do melhor que levo comigo!

Aos meus melhores amigos, Bea e Tiago! Amigos de quase sempre e para sempre, obrigada por fazerem parte da minha vida, por não me deixarem cair nunca, por acreditarem em mim sempre!

À Sara, Marta, Xana e à Inês, longe, mas sempre perto, muito obrigada por fazerem a minha vida tão mais feliz, pela preocupação, por me fazerem rir e descontrair!

À minha família, palavras também nunca chegarão para agradecer! Serão sempre o meu porto de abrigo e onde sou verdadeiramente feliz! O Bicho Libório não tinha chegado onde chegou sem vocês! Um especial obrigado e o mais importante à minha mãe! A ti devo-te tudo! Obrigada pela paciência, pelo apoio e amor incondicional, pela comida, por ser quem sou!

À minha mãe, ao meu pedacinho de céu e ao Tiago.

O trabalho apresentado nesta dissertação de tese foi realizado no Instituto de Investigação em Ciências da Vida e Saúde (ICVS), Universidade do Minho.

O financiamento para a realização deste projeto provém dos fundos do Programa Operacional Potencial Humano (POPH), do Programa Investigador FCT (IF) sobre a projeto IF/00959/2014. Os fundos do Programa Operacional Regional do Norte (NORTE 2020), sobre o Acordo de Parceria PORTUGAL 2020, através do Fundo Europeu de Desenvolvimento Regional (FEDER). O financiamento da FEDER advém também do Programa Operacional Fatores de Competitividade – COMPETE, e dos fundos nacionais através da Fundação para a Ciência e Tecnologia sobre POCI-01-0145-FEDER-007038; sobre o projeto NORTE-01-0145-FEDER-000013 e sobre o projeto POCI-01-0145-FEDER-028113.



STATEMENT OF INTEGRITY

I hereby declare having conducted this academic work with integrity. I confirm that I have not used plagiarism or any form of undue use of information or falsification of results along the process leading to its elaboration.

I further declare that I have fully acknowledged the Code of Ethical Conduct of the University of Minho.

Macrophages in pulmonary fibrosis: characterization and fibroblasts transdifferentiation modulation

Idiopathic pulmonary fibrosis (IPF) is the most common and lethal of interstitial lung diseases and affects around 3 million people worldwide. It is characterized by a progressive and irreversible loss of respiratory function due to lung architectural destruction. It is known that IPF comprises cycles of epithelial destruction, unbalanced formation of myofibroblasts and consequent excessive extracellular matrix deposition. Recent efforts have shifted the focus of uncovering the mechanisms of disease progression to understanding the role of inflammation, for instance pulmonary macrophages (MO) populations. In IPF, the roles of Alveolar (AMs) and Interstitial (IMs) macrophages described in literature are controversial. Thus, the main goal of this thesis was to contribute with new insights regarding whether AMs and IMs differentially modulate fibrosis progression through interactions with fibroblasts during the inflammatory phase. Bleomycin (BLM)-induced pulmonary fibrosis mouse model was used to study the proposed issues. First, MO characterization was performed by flow cytometry (FC), in the lung of untreated, BLM vehicle and BLM treated wild-type animals, at 3, 5, 7 and 9 days after its administration. We observed a progressive significant increase of IMs in treated animals. The expression of CD80, CD206 and MHCII was also assessed by FC and overall treated IMs present higher percentages of cells expressing these markers. Moreover, at day 7 after BLM administration, MO from untreated and treated mouse lungs cells were obtained by fluorescence activated cell sorting for further transcripts expression analysis of pro-inflammatory and anti-inflammatory genes, by qRT-PCR. Treated IMs showed increase of several genes that can potentiate their action in promoting a pro-fibrotic micro-environment. Secondly, to answer whether AMs and IMs are differentially regulating fibrosis progression, a mouse lung fibroblasts cell line was stimulated with MO conditioned media of MO separated by fluorescence activated cell sorting at days 7 and 9 after BLM administration. After stimulation, apoptosis, proliferation, metabolic activity and transdifferentiation state were assessed. Overall, 7th day IMs conditioned media stimulate higher levels of fibroblast transdifferentiation. Taken together, the findings of this thesis indicate that, in the peak of inflammatory phase (day 7), IMs population is the one crucial for promoting lung fibrosis progression.

Key words: alveolar and interstitial macrophages; fibroblast transdifferentiation; inflammatory phase

Os macrófagos na fibrose pulmonar: caracterização e modelação de transdiferenciação dos fibroblastos

A Fibrose pulmonar idiopática (FPI) é a forma mais comum e letal das doenças intersticiais pulmonares, afetando cerca de 3 milhões de pessoa no mundo. FPI é caracterizada pela perda progressiva/irreversível da capacidade respiratória como consequência da destruição da estrutura pulmonar. Sabe-se que a doença envolve ciclos de dano epitelial, acumulação exacerbada de miofibroblastos e consequente deposição excessiva de matriz extracelular. Mais recentemente o foco da investigação destas doenças tem sido a compreensão do papel da inflamação na sua progressão, como por exemplo das populações de macrófagos pulmonares (MO). As funções dos macrófagos alveolares (AMs) e intersticiais (IMs) que se encontram descritas na literatura são controversas. Assim, o objetivo principal desta tese foi contribuir com novos conhecimentos sobre se os AMs e IMs modulam diferencialmente a progressão da fibrose, nomeadamente através da interação com fibroblastos, durante a fase inflamatória, utilizando para tal o modelo de ratinho de fibrose pulmonar induzido por bleomicina (BLM). Primeiramente, a caracterização de MO foi realizada por citometria de fluxo (CF), no pulmão de ratinhos normais não tratados, tratados com o veículo da BLM e tratados com BLM, aos dias 3, 5, 7 e 9 após a sua administração. Os pulmões de ratinho tratados apresentaram um aumento significativo e progressivo na quantidade de IMs. Além disto, a expressão de CD80, CD206 e MHCII também foi verificada por CF, em que foi observado um aumento da expressão dos marcadores mencionados nos IMs tratados. No dia 7 após administração de BLM, os MO de células pulmonares de ratinhos tratados com BLM e não tratados foram obtidos por separação celular com recurso a CF para posterior análise de níveis de expressão de transcritos de genes associados à resposta pró-inflamatória e anti-inflamatória, por qRT-PCR. Observou-se o aumento da expressão de vários genes pelos IMs tratados, cuja ação está na sua generalidade associada à promoção de um microambiente pró-fibrótico. Em segundo lugar, e de forma a responder se os AMs e IMs modulam diferencialmente a progressão da fibrose por interação com fibroblastos, uma linha celular de fibroblastos de pulmão de ratinho foi estimulada com meio condicionado de MO, obtidos por separação celular com recurso a citometria de fluxo, nos dias 7 e 9 após a administração de BLM. Posteriormente, foi feita a análise de apoptose, proliferação, atividade metabólica e estado de transdiferenciação dos fibroblastos. Em geral, verificamos que nos ensaios *in vitro* de 7 dias, os meios condicionados derivados de IMs de animais tratados apresentavam maior capacidade de transdiferenciação de fibroblastos. Em conjunto, os dados desta tese indicam que, no pico da fase inflamatória (dia 7), a população de IMs é a população crucial na promoção da progressão da fibrose.

Palavras-chave: fase inflamatória; transdiferenciação de fibroblastos; macrófagos alveolares e intersticiais

Table of Contents

1. Introduction 15
   1.1. Idiopathic Pulmonary Fibrosis 15
      1.1.1. Diagnosis 16
      1.1.2. Therapy 17
   1.2. Pulmonary Fibrosis Pathogenesis 18
      1.2.1. Lung Epithelial Cells 20
      1.2.2. Myofibroblasts and their sources 21
      1.2.3. Inflammation 22
   1.3. Pulmonary Macrophages 22
   1.4. Pulmonary fibrosis mouse models 26
      1.4.1. Bleomycin-induced pulmonary fibrosis mouse model 26
2. Research Objectives 28
3. Material and Methods 29
   3.1. Experimental Design 29
   3.2. Animals 30
      3.2.1. Pulmonary fibrosis mouse model 30
   3.3. Lung Single Cell Suspension Preparation 31
   3.4. Flow cytometry 32
   3.5. Alveolar and Interstitial macrophages separation 35
   3.6. Reverse transcriptase quantitative polymerase chain reaction 37
   3.7. Cell Culture 38
      3.7.1. Primary Alveolar and Interstitial macrophages culture and collection of conditioned media 38
      3.7.2. MLg cell line 39
   3.8. *In vitro* assays 39
      3.8.1. Challenge of MLg cell line with conditioned media 39
      3.8.2. Viability curves 40
      3.8.3. Apoptosis assessment 40
      3.8.4. Immunofluorescence staining for fibroblasts proliferation and transdifferentiation 41
      3.8.5. Metabolic activity assessment (MTS) 42

3.9. Data analysis 42
4. Results 43
4.1. Characterization of macrophage populations during the inflammation phase of BLM-induced pulmonary fibrosis mouse model 43
4.1.1. Macrophage populations activation profile 45
4.2. Paracrine abilities of lung macrophage populations on fibroblast proliferation and transdifferentiation 51
4.2.1. Alveolar and Interstitial macrophages-derived conditioned media of 7 days after BLM administration 52
4.2.2. Alveolar and Interstitial macrophages-derived conditioned media of 9 days after BLM administration 58
5. Discussion 66
6. Conclusions and Future Perspectives 73
7. Bibliography 74
8. Annexes 82

List of abbreviations

A

ACK- Ammonium-Chloride-Potassium

AEC I- Alveolar epithelial type I cells

AEC II- Alveolar epithelial type II cells

AMs- Alveolar macrophages

APC- Antigen presenting cells

αSma- Alpha smooth muscle actin

Arg1- Arginase 1

ATS/ERS/JRS/ALAT- American Thoracic Society, European Respiratory Society Japanese Respiratory Society and Latin American Thoracic Association

B

BAL- bronchoalveolar lavage

BALF- bronchoalveolar lavage fluid

BLM- Bleomycin

BMDM- Bone marrow-derived macrophages

C

Ccl- CC chemokine ligand

Chi3l3- Chitinase-like 3

Ctgf- Connective tissue growth factor

Cxcl- CXC chemokine ligand

D

DAPI- 4,6-diamidino-2-phenylindole

DMEM- Dulbecco's Modified Eagle Medium

E

EMT- Epithelial-mesenchymal transition

ECM- Extracellular matrix

F

FBS- Fetal bovine serum

FC- Flow cytometry

Fn1- Fibronectin

FPI- Fibrose Pulmonar Idiopática

G

Gapdh- Glyceraldehyde-3-phosphate dehydrogenase

H

HRCT- High-resolution computed tomography

I

IPF- Idiopathic pulmonary fibrosis

ILDs- Interstitial lung diseases

IPF- Idiopathic pulmonary fibrosis

Il- Interleukin

Ifnγ- Interferon gamma

IMs- Interstitial macrophages

M

MDD- Multidisciplinary discussion

MEM- Minimum Essential Medium

MHCII- Major histocompatibility complex class II

Mmp- Metalloproteinases

MO- Macrophages

P

PFA- Paraformaldehyde

PBS1x- Phosphate Buffered Saline 1x

Pdgf- Platelet-derived growth factor

Q

qRT-PCR- quantitative real-time PCR

R

Retnla- Resistin like alpha

RT- Room temperature

S

SEM- Standard error of the mean

SMCs- Smooth muscle cells

SRB- Sulforhodamine B

T

Tgf-β- Transforming growth factor beta

Th1- T-helper type 1 inflammatory response

Th2- T-helper type 2 inflammatory response

Tnfα- Tumor necrosis factor alpha

U

UIP- Usual interstitial pneumonia

V

VD- Viable Dye

Vim- Vimentin

List of Figures

Figure 1 - Comparison of the 5-year survival (A) and death (B) rate for idiopathic pulmonary fibrosis (IPF) with different types of cancer..... 15
Figure 2 - Diagnosis algorithm for IPF..... 17
Figure 3 - Progression of Pulmonary Fibrosis. 20
Figure 4 - Model of developmental origin of lung macrophage diversity..... 23
Figure 5 - Time course for BLM-induced pulmonary fibrosis mouse model..... 27
Figure 6 - Experimental design of the thesis entitled "Macrophages in pulmonary fibrosis: characterization and fibroblasts transdifferentiation modulation". 29
Figure 7 - Gating strategy to identify AMs and IMs at 3, 5, 7 and 9 days after BLM administration in mice. 34
Figure 8 - Gating strategy to separate AMs and IMs at 7 and 9 days after BLM administration in mice. 37
Figure 9 - Determination of lung macrophage populations, AMs and IMs, quantity at four time-points (3, 5, 7 and 9 days) of the inflammatory phase of BLM-induced pulmonary fibrosis. 44
Figure 10 - Characterization of lung macrophage populations, AMs and IMs, activation profile at four time-points (3, 5, 7 9 days) of the inflammatory phase of BLM-induced pulmonary fibrosis. 47
Figure 11 - Transcript' expression analysis of pro- and anti-inflammatory mediators at day 7 after BLM administration..... 50
Figure 12 - Representative images of cell confluency and morphology observation in brightfield microscopy of mouse lung fibroblasts cell line after 48h stimulation with lung MO-derived conditioned media..... 53
Figure 13 - Assessment of fibroblast proliferative state after 48 hours of stimulation with lung MO-derived conditioned media. 55
Figure 14 - Assessment of metabolic viability of adherent cells, after 48 hours of stimulation with sorter lung MO-derived conditioned media..... 55
Figure 15 - Assessment of fibroblast transdifferentiation state after 48 hours of stimulation with lung MO-derived conditioned media. 58
Figure 16 - Representative images of cell confluency and morphology observation in brightfield microscopy of mouse lung fibroblasts cell line after 48h stimulation with lung MO-derived conditioned media..... 59
Figure 17 - Assessment of fibroblast proliferative state after 48 hours of stimulation with lung MO-derived conditioned media. 62

Figure 18 - Assessment of metabolic viability of adherent cells, after 48 hours of stimulation with sorter lung MO-derived conditioned media. 62
Figure 19 - Assessment of fibroblast transdifferentiation state after 48 hours of stimulation with lung MO-derived conditioned media. 65
Supplementary Figure 1 - MLg cell line is not able to growth in culture without media supplementation with FBS..... 82
Supplementary Figure 2 - Cell seeding density selection for *in-vitro* assays. 82
Supplementary Figure 3 - Characterization of macrophage population, AMs and IMs, dynamics at four time-points (3, 5, 7 9 days after BLM administration) of the inflammatory phase of pulmonary fibrosis using the gating strategy applied for the fluorescence activated cell sorting. 83

List of Tables

Table 1 - Groups and respective number of animals used and time-points after BLM administration for the experimental analysis. 31
Table 2 - Primary antibodies and respective concentrations used in flow cytometry staining protocol... 33
Table 3 - Primary antibodies and concentrations used in the flow cytometry staining protocol. 36
Table 4 - TaqMan® Gene Expression assays probes used in qRT-PCR analysis. 38
Table 5 - Primary and secondary antibodies used to assess fibroblast proliferation and transdifferentiation by immunofluorescence. 42
Table 6 - Summary of AMs and IMs percentages mean and standard error of the mean, in the animal groups tested at 4 time-points after BLM administration. 44
Table 7 - Summary of mean percentage of CD80, CD206 and MHCII positive AMs and IMs and standard error of the mean, in the animal groups tested at 4 time-points after BLM administration. 48
Table 8 - Summary of gene relative expression levels mean and standard error of the mean in sorted AMs and IMs from untreated and treated animals groups. 51
Table 9 - Quantification of Annexin V positive cells per DAPI positive cells of mouse lung fibroblasts, after 48h stimulation with lung MO conditioned media. 53
Table 10 - Summary of Ki-67 positive cells percentages mean and standard error of the mean in the tested conditions. 55
Table 11 - Summary of absorbance levels mean and standard error of the mean in the tested conditions. 56
Table 12 - Summary of Vim and αSma/Vim positive cells percentages mean and standard error of the mean in the tested conditions. 58
Table 13 - Quantification of Annexin V positive cells per DAPI positive cells of mouse lung fibroblasts cell line, after 48h stimulation with lung MO-derived conditioned media. 60
Table 14 - Summary of Ki-67 positive cells percentages mean and standard error of the mean in the tested conditions. 62
Table 15 - Summary of absorbance levels mean and standard error of the mean in the tested conditions. 63
Table 16 - Summary of Vim and αSma/Vim positive cells percentages mean and standard error of the mean in the tested conditions. 65

1. Introduction

Interstitial lung diseases (ILDs) comprise over two hundred heterogeneous parenchymal lung disorders that are associated with significant and increasing morbidity and mortality rates [1,2]. They all affect the lung interstitium, the tissue and space around the alveoli, and are characterized by variable degrees of inflammation and fibrosis [3]. Within this group, the most prevalent and lethal of ILDs is idiopathic pulmonary fibrosis (IPF) [4,5].

1.1. Idiopathic Pulmonary Fibrosis

IPF is a specific form of chronic, progressive fibrosing interstitial pneumonia, limited to the lungs, which cause remains unknown [5].

IPF prevalence increases significantly with age, with the majority of patients aged >50 years at diagnosis [6] and affecting a higher proportion of males than females [5,6]. Although there are no large-scale studies regarding IPF prevalence and incidence, epidemiological studies have estimated that this disease affect around 3 million people worldwide [4], with the population prevalence being 130,000 in the United States, 300,000 in Europe, 640,000 in East Asia [4]. It is reported that IPF incidence is increasing worldwide and that is similar to the ones of stomach, liver, testicular and cervical cancers [7]. Patients' survival is variable and the median survival is estimated to be 3-5 years, after diagnosis [5]. The rate of survival is similar or even worse than several types of cancer, as demonstrated in Figure 1 [8].

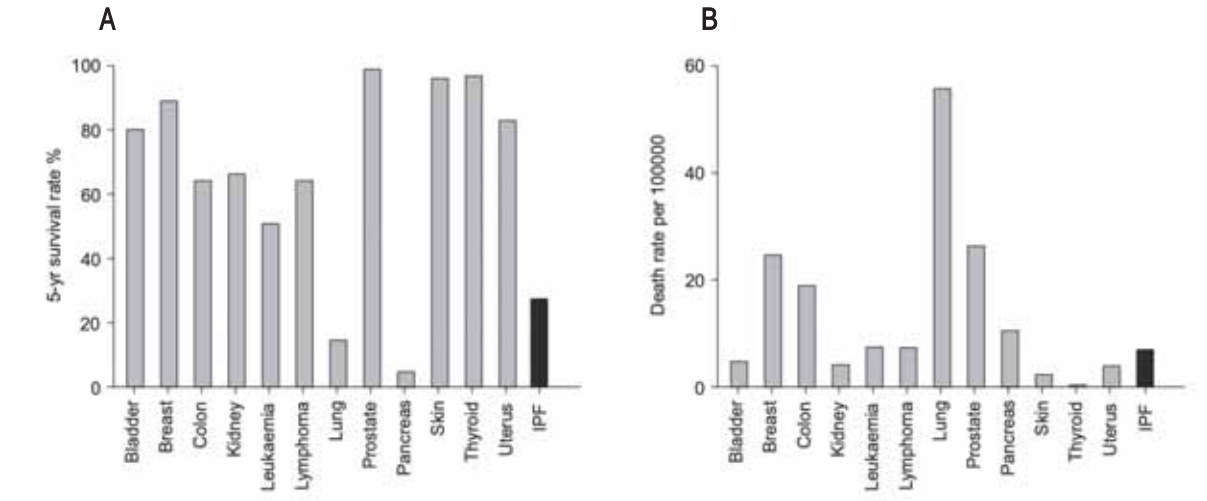


Figure 1 - Comparison of the 5-year survival (A) and death (B) rate for idiopathic pulmonary fibrosis (IPF) with different types of cancer. Adapted from Vancheri et al. 2010 [8].

This fatal disease as an unpredictable and heterogeneous behavior. Although the majority of patients demonstrates a gradual worsening of lung function, there is also a group of patients that remains stable and then declines very rapidly [5]. However, is it difficult to predict the rate of progression in individual patients [9]. Disease progression is seen by worsening of respiratory symptoms, decline in pulmonary function test results, progressive fibrosis, acute respiratory decline, or death. Most IPF patients present comorbidities such as pulmonary hypertension, gastroesophageal reflux, obstructive sleep apnea, obesity and emphysema, that have a negative impact in the disease [5].

Despite the unknown etiology, several potential risk factors have been associated with IPF namely, age, sex, tobacco smoking, environmental exposures (farming, livestock, wood dust, metal dust, stone dust and silica), microbial agents (chronic viral infections), abnormal gastroesophageal reflux and genetic predisposition (polymorphisms in genes encoding several cytokines, profibrotic molecules, surfactant proteins, immunomodulatory genes) [5].

1.1.1. Diagnosis

Clinicians should consider IPF in all adult patients that, upon examination, present unexplained chronic exertional dyspnea, chronic dry cough, bibasilar inspiratory crackles and digital clubbing [5]. In practice, early recognition and accurate diagnosis are still a problem, as many of these patients initially receive a diagnosis of heart failure or chronic obstructive pulmonary disease. This suggests that clinicians often fail to consider ILDs which will jeopardize patient outcome [10].

According to the 2018 American Thoracic Society, European Respiratory Society Japanese Respiratory Society and Latin American Thoracic Association (ATS/ERS/JRS/ALAT) guidelines, the diagnosis pathway of IPF, highlighted in figure 2, requires the exclusion of other known causes of IDLs, through a careful patient history and physical examination focusing on comorbidities, medication use, environmental exposures and family history [11]. In the absence of an identifiable/certain cause, the diagnosis pathway follows with a high-resolution computed tomography (HRCT) to determine whether the disease is present by identifying the hallmark pattern of IPF, the usual interstitial pneumonia (UIP). The histopathological UIP pattern is characterized by areas of marked fibrosis, fibroblast foci, architectural distortion, presence of patchy involvement of the lung parenchyma and honeycombing [5,12,13]. Honeycombing is a key characteristic of the UIP pattern, and its presence is required for a definite radiological diagnosis. It is defined as clustered, thick cystic spaces with well-defined walls of similar diameters in a predominantly

sub-pleural/paraseptal distribution, that can be accompanied by a traction bronchiectasis (chronic condition where the walls of the bronchi are thickened) or bronchiolectasis (dilatation of bronchioles) [5,11,13]. Four diagnostic categories that incorporate the HRCT features are established: UIP pattern, probable UIP pattern, indeterminate for UIP pattern and alternative diagnosis. A clear UIP pattern establishes a diagnosis of IPF. For patients that have a HCRT pattern of probable UIP, indeterminate or an alternative diagnosis is recommended cellular analysis of their bronchoalveolar lavage (BAL) fluid, which may help to distinguish IPF from some alternative ILDs, and a surgical lung biopsy [11]. However, is often not possible to have the histological confirmation of IPF through lung biopsy due to disease severity and patient comorbidities [13]. A multidisciplinary team of clinicians, radiologists and pathologists' experts in IPF is always recommended for an increased accuracy in IPF diagnosis and a higher prognostic significance [4,5,11].

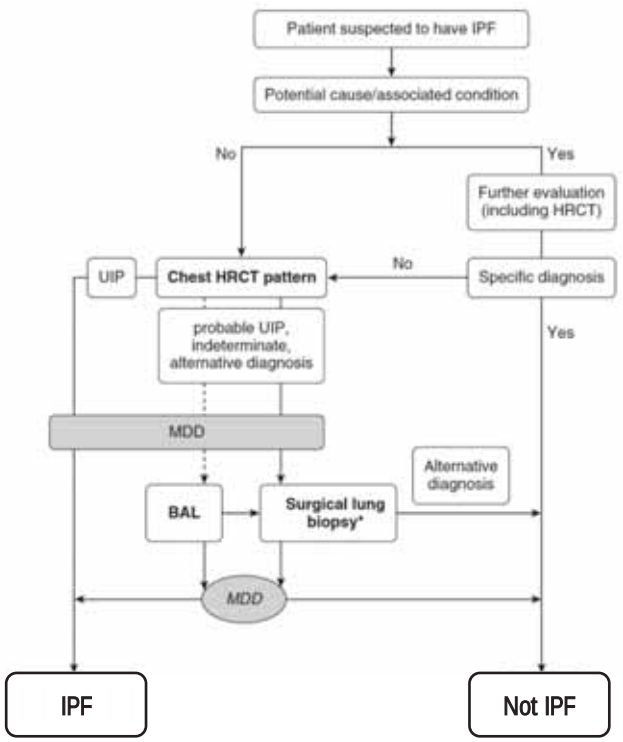


Figure 2 - Diagnosis algorithm for IPF. Adapted from Raghu et al 2018 [11].

1.1.2. Therapy

IPF management focuses on the attempt of symptoms amelioration, health status improvement, lung function preservation, minimization of adverse effects of therapy and, ideally, survival improvement [4], since there is no cure.

Until 2014, IPF treatment was focused on immunosuppressant therapy, supplemental oxygen and supportive care [14]. In 2015, the ATS/ERS/JRS/ALAT updated the therapy guidelines, making strong and conditional recommendations for and against certain treatments [15].

The treatment that combined prednisone (a corticosteroid), azathioprine (an immunosuppressive) and N-acetyl cysteine (a mucolytic) was widely regarded as the standard of care for IPF worldwide. With the new guidelines, this treatment is now strongly not recommended due to its association with an increased risk of hospitalization and death [15]. Also, chronic use of immunosuppressants is no longer recommended [14]. Nintedanib and pirfenidone clinical trials showed to slow lung function decline and were approved by the US Food and Drug Administration in 2014. Both drugs are believed to inhibit essential fibrosis pathways [14]. Nintedanib inhibits tyrosine kinases, including the fibroblast growth factor receptor, platelet-derived growth factor receptor, and vascular endothelial growth factor receptor. It was shown that this drug slows lung-function decline and acute exacerbations in IPF patients [16–18]. Pirfenidone is an orally bioavailable synthetic molecule which mechanism of action in IPF is not completely understood [19]. Despite this, it has been studied in several clinical trials and the data shows that this drug also slows lung-function decline [19,20]. ATS/ERS/JRS/ALAT 2015 guidelines recommended the potential use of both drugs, with the indication that the majority of patients should benefit from those treatments, but each patient situation should be carefully evaluated [14,15]. When medical options are no longer available, lung transplantation is the only treatment considered, by having the potential to improve quality of life and survival of IPF patients [4].

Despite the advance in IPF treatment in recent years, IPF continues to be a progressive heterogeneous disease with poor prognosis, which pathobiology understanding is still very limited. An increase in knowledge of the crosstalk between disease mechanisms and key cellular players will be undoubtedly crucial to reach this purpose. Thus, gaining new knowledge regarding IPF pathogenesis is essential to find potential therapeutic targets.

1.2. Pulmonary Fibrosis Pathogenesis

Pulmonary fibrosis occurs when normal lung tissue is replaced by scar tissue. Consequently, pulmonary architectural is damaged, leading to impairments in gas exchange, reduction in blood oxygenation and respiratory insufficiency, which is often lethal [14,21].

For many years IPF was defined as an inflammatory disease due to the increase in inflammatory cells in lung [4,22]. However, this hypothesis was left aside, and the current paradigm suggests that the disease is

an epithelial-driven disease (Fig. 3A) [4]. Thus, a dysfunctional ageing epithelium is exposed to repeated micro-injuries that lead to defective attempts of regeneration and initiate dysregulated repair cycles [13,22,23]. Thus, a fibrotic environment is established [13,22]. Subsequently, occurs damage and destruction of the alveolar capillary basement membrane, which allows the infiltration of fibrogenic cells from the alveolar interstitium and recruitment of the inflammatory component, such as macrophages (MO) and neutrophils (Fig. 3B) [21]. It is though that growth factors secreted by the injured epithelial cells and inflammatory cells, promote fibroblast and fibrocytes recruitment, proliferation and differentiation into active myofibroblasts [4]. These cells are considered to be key effectors of pulmonary fibrosis. The cycles of abnormal wound-healing sustain the formation of fibroblastic foci, disordered type II alveolar epithelial cells in association with fibroblasts/myofibroblasts, that is considered a key histological feature of the UIP pattern [14,24,25]. These myofibroblasts secrete exaggerated amounts of extracellular matrix (ECM) components [4]. Along with excessive ECM production and unorganized accumulation occurs the aberrant lung remodeling through bronchiolization of the alveolar tissue, in which the airway basal cells may function as stem cells and contribute to re-epithelization of damaged alveolar epithelium (Fig. 3C) [22,26]. This culminates in lung tissue remodeling/scaring, destruction of the normal lung architecture and gradually loss of function [4,13].

One of the most important and studied molecular players in IPF pathogenesis is transforming growth beta (Tgf-β). This growth factor is secreted by epithelial cells, immune cells, such as MO, and by fibroblasts. It promotes epithelial cell apoptosis, epithelial-mesenchymal transition, epithelial cell migration, production of other profibrotic mediators and recruitment of fibroblasts and circulating fibrocytes and their activation, proliferation and transformation into myofibroblasts.

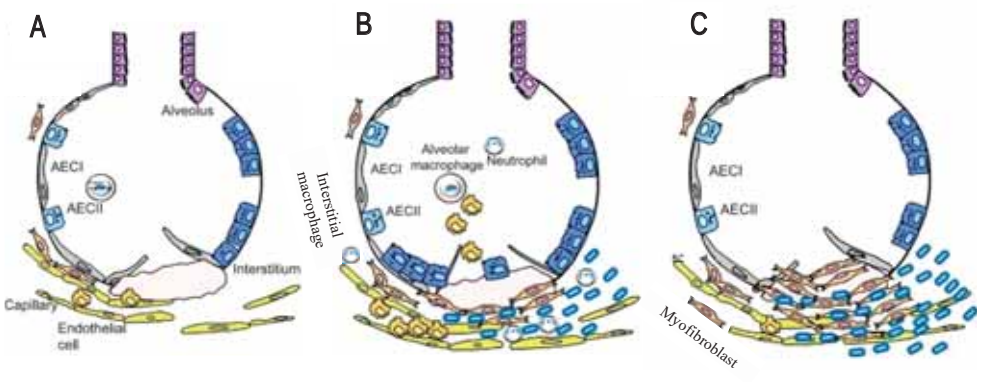


Figure 3, legend on next page

Figure 3 - Progression of Pulmonary Fibrosis.

The onset of pulmonary fibrosis is characterized by cycles of injury that occur in a susceptible epithelium (A) that promote destruction of the alveolar structure, production of inflammatory mediators and consequent recruitment of inflammatory cells, such as neutrophils and macrophages (B). This is accompanied by an abnormal repair process, with an abnormal re-epithelialization, abundance of myofibroblasts and the formation of a collagen matrix (C). The continuous cycles of injury, dysregulated repair and excessive extracellular matrix deposition culminate in lung architecture distortion and loss of function (C). Adapted from Wuyts et al. 2013.

1.2.1. Lung Epithelial Cells

In a normal lung, both in mice an in humans, the alveolar compartment is constituted by two types of pneumocytes, alveolar epithelial type I cells (AEC I) and alveolar epithelial type II cells (AEC II). AEC I cells cover 90 to 95% of the alveolar surface, having their basement membrane fused with endothelial cells, to allow a correct gas exchange. These cells form a barrier that is able to sense microbial products and stimulate an inflammatory response. AEC II cells cover the rest of the alveolar surface and are responsible for the synthesis and secretion of pulmonary surfactant. Also, a subpopulation of AEC II function as alveolar stem cells that can differentiate into AEC I cells during alveolar homeostasis and in post injury repair [27–29].

The alveolar epithelial balance is loss in the lung of IPF patients. It is thought that the continuous exposure to micro-injuries leads to AEC I cells damage. AEC II cells should regenerate the damaged AEC I compartment, which is not correctly observed once the former are abnormally activated [22]. This is translated into AEC II hyperplasia, apoptosis, senescence and partial epithelial-mesenchymal transition (EMT) with formation of myofibroblasts. These characteristics were already observed in lung tissue from IPF patients, within fibroblastic foci [30–32]. In parallel with altered characteristics, these dysfunctional epithelial cells also produce mediators that contribute to the expansion of fibroblast and myofibroblast population, as well as to the remodeling of the ECM and inflammatory cell recruitment. Among these mediators are several metalloproteinases (Mmp), chemokines, platelet-derived growth factor (Pdgf), interleukin (Il)-1β , Il-6, Il-13, Tgf-β [4,22,33]. Interestingly, abnormally activated epithelial cells recapitulate embryological pathways through the expression of WNT-pathway components and Sonic Hedgehog [34]. These pathways crosstalk with Tgf-β and activate a pro-fibrotic feedback loop [34].

1.2.2. Myofibroblasts and their sources

The contribution of mesenchymal cells to IPF pathogenesis is crucial as the key effector cells of fibrosis are myofibroblasts [35]. These are contractile fibroblastic cells that share features of both fibroblasts and smooth muscle cells (SMCs). Myofibroblasts have contractile capacity, gained by expression of alpha smooth muscle actin (αSma) [36,37] and are responsible for the enhance ECM synthesis. The ECM produced by these cells during fibrotic process in poorly organized but very dense. It is thought that both the altered composition and quantity of ECM as well as its stiffness may contribute to the disease pathogenesis, by creating cycles of positive feedback loop between fibroblasts and the aberrant ECM, in which the fibrotic ECM is both a cause and a consequence of fibroblast activation [4,22,38]. The exact mechanisms of how this works remain unclear.

Myofibroblasts sources are proposed to include resident fibroblasts, circulating fibrocytes and epithelial-mesenchymal transition. Resident fibroblasts are found in the lung interstitium and are cells committed to maintain and restore a normal and well-structured ECM in wound healing responses [39]. During IPF pathogenesis, fibroblasts within the fibrotic foci assume a migratory, proliferative and ultimately profibrotic phenotype which leads to significant increase in ECM production and their transdifferentiation into active myofibroblasts [22,37]. This fibroblastic alteration of phenotype occurs in response to growth factors including Tgf-β, Pdgf-β and connective tissue growth factor (Ctgf), which are produce by the damaged epithelium as well as inflammatory cells [37]. Fibrocytes were first identified as circulating bone-marrow derived progenitor cells that migrate into wounds and participate in the repair [4,37]. In IPF, upon tissue injury and in response to chemotactic factors, such as Tgf-β, fibrocytes migrate to the lung and differentiate in fibroblast-like cells and myofibroblasts [40,41]. It is thought that these cells contribute to tissue remodeling and fibrosis with several functions, besides the ECM production, such as fibroblast activation and alternative MO-dependent and -independent inflammatory processes [40]. Higher levels of fibrocytes have already been identified in the peripheral blood of IPF patients [42]. EMT is the third source of myofibroblasts in IPF. This process can occur by molecular reprogramming of the AEC II cells, in response to pro-fibrotic mediators and microenvironment [22]. Epithelial cells down-regulate their typical markers and start to express mesenchymal cell associated genes, lose contact adhesion to the basement membrane, alter their shape in association with cytoskeletal changes and acquire some mesenchymal features of invasion, migration and ECM production [43].

1.2.3. Inflammation

Inflammatory processes and cells are involved in normal wound healing processes since the early stages [22]. Regarding IPF, despite the role of inflammation remaining controversial, it is clear that inflammatory mediators play important roles in progression of the disease [44]. It is though that both innate and adaptive immune cells modulate fibrogenic processes [33]. The cycles of epithelial injury can cause an imbalance in T-helper type 1 (Th1)/type 2 (Th2) inflammatory response [36]. Epithelial cells release factors such as Il-25, Il-33 that facilitate the development of profibrotic Th2 responses. In turns Th2 cells produce Il-4 and Il-13 that induced the recruitment of neutrophils, mast-cells, eosinophils, mesenchymal cells, more macrophages progenitors that once in the injured environment acquire a pro-fibrotic phenotype and production of Tgf-β by the injured epithelium and recruited inflammatory cells [21,22]. The interleukins produce by a Th2 response promote the development of a profibrotic macrophage subpopulation that secretes Tgf-β and contributes to the fibrotic process [21]. Recruited neutrophils produce various proteases, particularly neutrophil elastase and metalloproteinases, which degrade matrix components but can also activate Tgb-β, thereby promoting ECM accumulation [36]. The Th2 immune response also contributes to a failure of correct re-epithelialization as well as fibroblast migration to the site of injury, promoting their proliferation and differentiation into myofibroblasts [21].

1.3. Pulmonary Macrophages

Mo play important roles in tissue repair and immunity of several organs, through their phagocytic and scavenger capacities as well as their highly plastic phenotypes, which allows them to shift their activation profile, in respond to environmental cues and molecular mediators [45].

In a healthy lung, MO represent the most abundant immune cell population [46]. Two main resident MO sub-types are found: Alveolar macrophages (AMs) that mostly reside in the airways and Interstitial macrophages (IMs), mostly localized within the lung parenchyma [47,48]. The current premise is that MO of different origins colonize the lung in three successive waves during development, with each population throughout different localizations in the lung (Fig. 4) [49]. Resident AMs were shown to originate from precursors that arise during embryogenesis and populate the lung around birth [49]. In a steady state, this MO population can self-maintain, with minimal contributions from bone marrow-derived macrophages (BMDM) [46], and are characterized by the expression of high levels of Siglec-F, with fluctuant levels of CD11b expression [50]. However, following irradiation or inflammation, BMDM significantly contribute to

AMs re-establishment [46]. AMs have several known functions, including maintenance of immunologic homeostasis and host defense by doing through turnover of surfactant, efferocytosis, defense removal of foreign particles and pathogens [51,52]. The analysis of lung myeloid compartment was, for a long time, mostly limited to the macrophages present in the airways. Thus, the AMs population is much more well studied and understood than IMs [47,53]. The phenotypic characterization of lung immune cell has been improving substantially with the evolution of methods that allowed harvest of tissue pulmonary macrophages and analysis of freshy isolated single cells [53]. IMs ontogeny is still not completely understood, partially due to the mentioned difficulties in identifying and isolating this MO population [46,47]. It is thought that IMs have a mix origin, both derived from embryonic yolk sac origin and postnatal bone marrow origin [49,53]. Parabiosis studies have suggested that in adulthood, IMs maintenance is, at least in part, accomplished by e replenishing from blood monocytes [47]. IMs roles are thought to have regulatory functions within the lung tissue, being involved in tissue remodeling and maintenance [49]

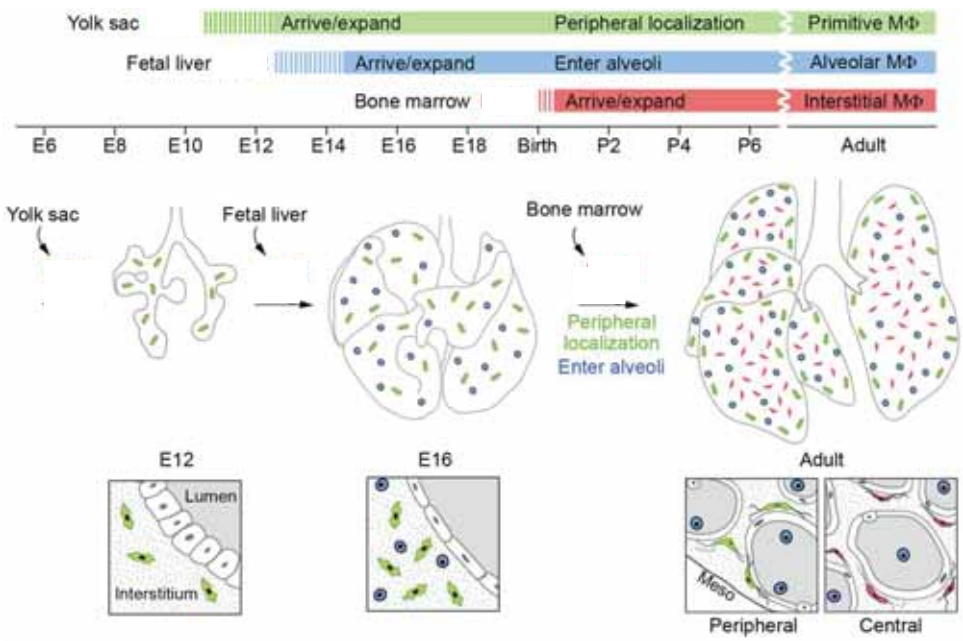


Figure 4 - Model of developmental origin of lung macrophage diversity.

In the first wave, embryonic MO (green) arrive from yolk sac. Then, another population of embryonic MO starts arriving two days later (blue). These MO are thought to be from fetal liver origin. During the first week of postnatal life, the MO derived from the second wave, enter the lumen and become AMs, which have the capacity to self-renew. MO derived from the first wave persist at specific location and give rise to the so-called IMs, In the parenchyma, a new population of definitive IMs arises from circulating monocytes of bone marrow origin. Adapted from Tan et al. 2016 [49].

MO are known to be integrated in all stages of the fibrotic process, having the capacity to both promote and inhibit its development [44]. In a study of liver fibrosis, it was observed the reduction in tissue scarring and myofibroblasts levels, when MO were depleted during the early inflammatory/maintenance phase of a fibrotic response. In contrast, when the depletion of MO was performed during the late remodeling/recovery phase, fibrosis persisted [54].

Growing evidence support the role of pulmonary MO in the pathogenesis of IPF [48,55,56]. These cells are often found in close proximity to fibrogenic sites and are thought to contribute to chronic inflammation that promotes progressive fibrosis [48]. MO are suggested as regulators of fibroblast recruitment, proliferation transdifferentiation and ECM production, as they produce several profibrotic mediators, including Tgf-β and Pdgf that induce those changes in fibroblasts [57]. They also promote fibrosis by secreting chemokines and matrix metalloproteinases which degrade ECM and facilitate the continuous recruitment of inflammatory cells to the sites of tissue injury [44]. MO can also inhibit fibrosis by inducing myofibroblast apoptosis, digesting and engulfing ECM components and by stimulating the production of collagen degrading MMP by a variety of cell types, including neutrophils [58].

As highly plastic cells, macrophages can assume transient phenotypes that promote or revolve fibroproliferative responses to tissue injury. MO have been characterized by the M1/M2 paradigm, in which classically activated M1 macrophages arise in response to interferon gamma (Ifnγ) and tumor necrosis factor alpha (Tfnα) and in response produce proinflammatory cytokines, mediate resistance to pathogens, induce myofibroblasts apoptosis and produce Mmp that contribute to ECM degradation. In contrast, M2 MO arise in response to IL-4, IL-10, IL-13, and Tgf-β1 stimulation and are involved in the aberrant wound-healing cascade during fibrosis, due to their capacity to produce pro-fibrotic cytokines like Il-4, Tgf-β and Il-10 [57]. This paradigm is increasingly put into question because the extent of MO activation if likely to be a very dynamic process and a sliding scale of activation, instead of being terminally differentiated, as these cells can express both M1 and M2 at the same time and the expression is altered in response to the disease context [59].

Recent studies the are pinpointing roles of the specific MO populations, AMs and IMs, in different forms of fibrogenesis [48]. In studies using human data, the information regarding IMs are scarce, probably due to the difficulties in identifying and obtaining these cells to study. In a recent study, the investigators obtained IPFs and normal lung tissue and observed a significant expansion of a subpopulation of MO in IPF lung [60]. This population was only found in the interstitial compartment of the lungs, indicating that could be an increase in IMs [60]. Regarding AMs, a single-cell RNA-Seq study and immunohistochemistry observed differentially expressed pro-fibrotic genes between fibrotic compared with normal lungs and that

normal lungs did not stain for the several pro-fibrotic markers analyzed [61]. Moreover, several studies indicate that AMs from IPF patients, mostly retrieved from BAL, have increased M2-like phenotype [48,59,62]. The majority of the results are controversial and indicate contradictory functions for these populations during the IPF pathogenesis. Namely, using bleomycin-induced pulmonary fibrosis mouse model, a study reported that $Ly6C^{hi}$-monocyte-derived AMs is driving fibrosis, where it was observed a rapid expansion of circulating $Ly6C^{hi}$ monocytes which peaked at day 3 after bleomycin challenge and that was followed an increase in AMs ($F4/80^{+}CD11c^{+}CD206^{+}$) that peaked at day 14 [63]. There were no significant alterations found in IMs ($F4/80^{+}CD11c^{-}CD206^{+}$) [63]. Another two studies using the same model found that monocyte to alveolar macrophage differentiation unfolds continuously over the course of fibrosis [50,64]. It was observed that during the acute inflammatory phase, at day 5, the number of AMs ($CD64^{+}Siglec\text{-}F^{+}$) significantly decreased, while the number of IMs ($CD64^{+}Siglec\text{-}F^{-}$) increased [64]. In contrast, Misharin et al 2017 showed that during the fibrotic phase, at day 21, AMs number was higher in treated animals than in control, while the IMs population returned to levels similar to the control [50,64]. Moreover, the increased AMs population results from recruitment and differentiation of circulating monocytes [50]. The difference in quantity of AMs and IMs during the different phases of the disease (inflammation and fibrotic phase) could indicate that these populations have different roles in the different time-points of the disease. These differences in quantity of AMs of IMs were not addressed in the work, thus remaining unanswered if the differences are translated into altered functions during disease progression. Interestingly, in the same work of Misharin et al 2017, monocytes, IMs, monocyte derived-AMs, and tissue resident AMs were obtained by fluorescence activated cell sorting, at 14 and 19 days after BLM administration and their gene expression analyzed using RNA-seq [50]. It was observed that a cluster of genes associated with fibrosis progression were differentially expressed and increased in IMs and monocyte derived-AMs [50]. In another report, $Gr1^{-}$ IMs were identified as the pulmonary macrophages population necessary to the development of radiation-induced fibrosis [65]. Overall these discrepancies may be partially explained due to, among studies, the use of different surface markers to characterized AMs and IMs and their profile characterization, as well as the time-points chosen to analyze these populations are not maintained across studies. For these reasons, it is clearly necessary a broader characterization of pulmonary macrophages and their activation phenotypes that allows the understanding of the population's states and changes across the different phases of the disease progression.

1.4. Pulmonary fibrosis mouse models

Several animal models have been developed to investigate the key mechanisms underlying the pathogenesis of pulmonary fibrosis and ultimately identify potential therapeutic targets. Despite the fact that none of animal models can completely recapitulate all features of human IPF, the use of animal models has allowed the reproduction of many key features of IPF. Among these models are instillation of bleomycin, fluorescein isothiocyanate, asbestos and silica; transgenic mice; irradiation model. The most extensively used and best characterized mouse model is the bleomycin induced pulmonary fibrosis mouse model [66,67].

1.4.1. Bleomycin-induced pulmonary fibrosis mouse model

Bleomycin (BLM) was first isolated from *Streptomyces verticillatus* and was found to be effective a squamous cell carcinomas and skin tumors. For this reason, its primary clinical use was as a chemotherapeutic antibiotic. BLM usefulness as an anti-neoplastic agent was discovered to be limited because it induced dose-dependent toxicity that resulted in fibrosis. This toxicity was observed predominantly in organs such as the lung, skin and mucous membranes due to the lack of bleomycin hydrolase in those tissues, the enzyme that inactivates BLM. The levels of this enzyme are particularly low in the lung when compared to other organs, which leads to greater susceptibly of BLM action and enables the persistence of the compound, leading to pulmonary fibrosis [66–68].

Several pathological features of human pulmonary fibrosis are reproduced in this model, such as epithelial cell injury and reactive hyperplasia, induction of lung parenchymal inflammation and interstitial and alveolar fibrosis [69,70]. In this mouse model, BLM is thought to induce lung injury via its ability to cause DNA strand breakage and oxidative stress [66]. The time course of the disease in this model is illustrated in figure 5. This model is characterized by dominance of inflammatory reaction during the first week post-BLM administration, due to widespread damage to the epithelium. In this inflammatory phase occurs an influx of inflammatory cells and consequent significant increase in production of pro-inflammatory cytokines such as Il-1, Tnf-α, Il-6 and Inf-γ [71]. At around day 9 post-BLM administration the inflammation vanishes gradually and is accompanied increase in by fibroblast proliferation, initiation of myofibroblast emergence and excessive extracellular matrix deposition [71,72].

The “switch” between inflammation and fibrosis promotes the increase in expression of pro-fibrotic markers, like Tgf-β, fibronectin (Fn1) and procollagen-1 [71]. By day 14 the fibrotic phase, the changes in

tissue and cell dynamics can be detected biochemically and histologically [68]. The fibrosis phase reaches its maximal responses between days 21 and 28 [69,71]. Some reports state that the fibrotic lesions resolve after 21 to 28 days [66,73]. This is seen as a disadvantage of this model, as it doesn't recapitulate the irreversible characteristic of the disease pathogenesis observed in IPF.

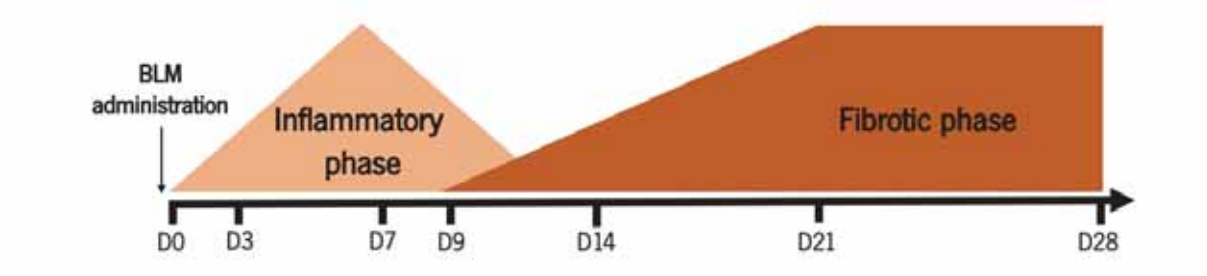


Figure 5 - Time course for BLM-induced pulmonary fibrosis mouse model.

Administration of BLM is followed by an inflammatory reaction, which start to disappear after a week and is replaced by a fibrotic onset.

2. Research Objectives

Understanding IPF pathogenesis is essential to find potential therapeutic targets that will allow improvement in patient quality of life. An increase in the knowledge of the crosstalk between key cellular players, such as macrophages and fibroblast/myofibroblasts, will be undoubtedly crucial to reach this purpose. Furthermore, the data regarding the functions of the two MO populations in IPF is very controversial thus not allowing the correct understanding of AMs and IMs roles during fibrosis. In this way, our main goal was to bring new insights into whether AMs and IMs differentially modulate fibrosis progression, more specifically during the inflammatory phase of the disease, namely through interactions with fibroblasts/myofibroblasts.

To accomplish the main goal, this work intended to:

1. Characterize the lung macrophage populations and their activation profile during the time-course of the inflammatory phase of BLM-induced pulmonary fibrosis;

2. Understand the paracrine abilities of the two main lung MO populations, AMs and IMs, on fibroblast proliferation and fibro-myofibroblast transdifferentiation.

3. Material and Methods

3.1. Experimental Design

The timeline for the experimental procedures performed in this thesis, respective animal groups, time-points of analysis and used techniques are explained in the next sub-sections and is represented in Figure 6.

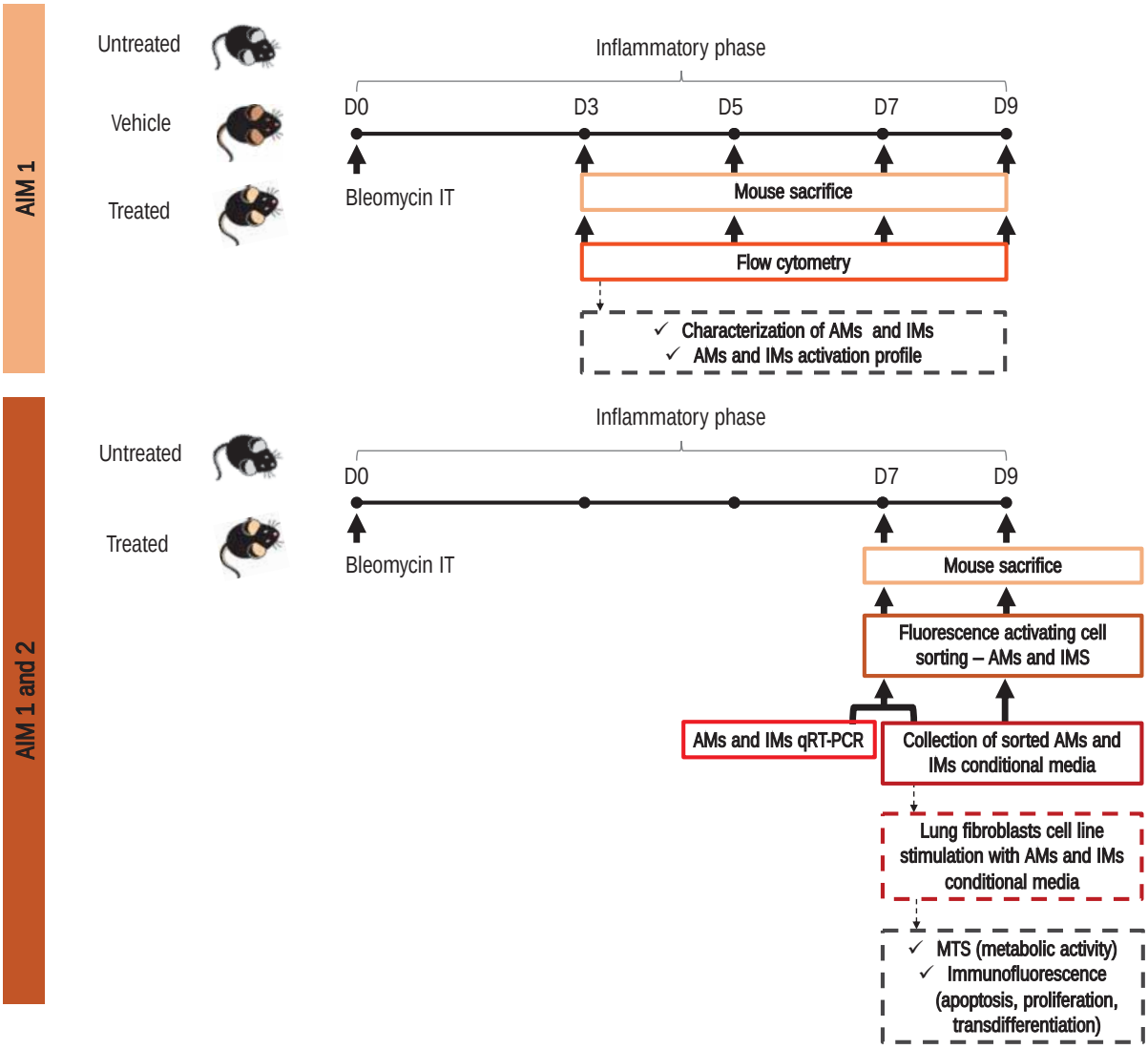


Figure 6 - Experimental design of the thesis entitled "Macrophages in pulmonary fibrosis: characterization and fibroblasts transdifferentiation modulation".

3.2. Animals

All animal experiments were approved by the Ethical Subcommittee in Life and Health Sciences (SECVS; ref. SECVS-032/2017) and performed accordingly to the European Union Directive 2010/63/EU. C57BL/6J mouse strain, supplied by Charles River, was used in the experiments. This colony was kept inbreed (WT mice mating) and in pathogen specific-free conditions. Animals were maintained in standard controlled environment (55% of humidity, 22-24°C, 12h light's cycle, food and water *at libitum*) and housed in proper cages (267 x 207 x 140 mm; five animals per cage).

3.2.1. Pulmonary fibrosis mouse model

Ten- to twelve-week-old male mice were used to induce pulmonary fibrosis using the well-known and established bleomycin-induced lung injury [66,67]. Two days before the surgery, animals were handled to be identified and weighed, as well as, to reduce the stress induced by the surgical procedures. Hence, for these procedures, first analgesia was administrated via a buprenorphine (0.3 mg/kg, Bupac, Richer Pharma, AG, Austria) subcutaneous injection. After fifteen minutes, animals were anesthetized via intraperitoneal injection of ketamine (75mg/kg, Ketamidor, Rochester Pharma, AG, Austria) and medetomidine (1mg/kg, Dormitor, Pfizer, USA). With animals under the effect of anesthesia, a small incision on the throat region allowed access to the tracheal rings. Then, a single dose of bleomycin (BLM) sulphate (2.0mg/kg; BML-AP302-0010, Enzo Life Sciences) or the drug vehicle, saline solution, was administrated via intratracheal injection, using a 30G needle. In order to revert the anesthesia effect, a subcutaneous injection of atipamezole (1mg/kg, Orion Corporation, Finland) was provided. Surgical procedure day was considered as day 0.

After the procedure, animals were followed closely, in order to insure the complete recovery from the surgery. During the recovery period, animals were housed in their cages, humidified food was placed on the cage's floor. After, a daily monitorization was performed to assess breathing, weight, fur, healing aspect and animals' movement/posture. Humane endpoints were established as respiratory difficulties and 20% weight loss during all the experiment period.

At 3, 5, 7 and 9 days, three experimental groups were used for flow cytometry analysis: Untreated group – animals that do not undergo surgical procedure and are used to obtain the population of interest in normal homeostatic conditions; Vehicle group - animals administered with saline solution and are used to understand if the drug vehicle is inducing alterations; Treated group - animals administered with BLM

and are used to study the populations of interest in disease context. Moreover, a second set of untreated and treated animals was used at 7 and 9 days to primary cell culture and conditioned media collection. A third set of untreated and treated animals was used at day 7 to separate AMs and IMs for transcripts expression analysis. Number of animals considered for each set of experiments is described in Table 1. In all animal sets mentioned, one independent experiment was conducted.

At 3, 5, 7 and 9 days after BLM administration, animals were sacrificed via an anesthesia overdose. Bronchoalveolar lavage fluid (BALF) was collected, following by transcardially perfusion with Phosphate Buffered Saline 1X (PBS1x). Following body perfusion, lung tissue dissociation was performed, as described below.

Table 1 - Groups and respective number of animals used and time-points after BLM administration for the experimental analysis.

Analysis	Days after BLM	Animals group		
		Untreated	Vehicle	Treated
Flow cytometry	3	4	4	7
	5	4	4	7
	7	4	7	10
	9	4	5	8
Fluorescence activated cell sorting	7	10 / 5 *	-	9 / 5 *
	9	9	-	7

*The first set of animals (10 untreated and 9 treated) was used to further qRT-PCR analysis and the second set of animals (5 untreated and 5 treated) was used to primary cell culture and further conditional media collection.

3.3. Lung Single Cell Suspension Preparation

Exposition of the tracheal rings allows trachea cannulation with a 25G needle associated to a syringe with 1 mL of PBS1x. Lungs were injected and aspirated with this solution and the process was repeated three times. We were able to recover 80 to 90% of fluid withdrawal. After collection, BALF was maintained on ice to be then added to single cell suspensions obtained from tissue dissociation, explained below.

After BALF collection and body perfusion, lungs were removed from the rib cage and placed in a petri dish with dispase (11553550, Corning) while minced into small pieces of 2-3 mm^2, for 20 min at room temperature (RT). Following this, DNase I (10104159001, Roche) and collagenase II (17101-015, Gibco) solution (DNase I 1 mg/mL and Collagenase II 5 mg/mL in Dulbecco's Modified Eagle Medium – DMEM;

21969-035, Gibco) was added to promote enzymatic digestion, for 10 min at 37°C. After these 10 min, mechanical tissue disruption was performed by titration with P1000 tip and the samples were incubated again for 10 min at 37°C. After the second incubation, mechanical tissue disruption was performed again. On ice, disrupted tissue suspensions were collected and discarded through 100 μm cell strainer placed on a 50 mL tube. To certify the recovery of maximum cells, petri dishes were washed with DMEM/20% fetal bovine serum (FBS, 10270-106, Gibco) and the liquid was also discarded through the cell strainer. The tissue that remained in the cell strainer was mechanically dissociated using the black back of a 10 mL syringe. After this, cell strainer was washed with DMEM/20% FBS. Then, the obtained suspension was discarded through a 70 μm cell strainer which was then washed with DMEM/20% FBS. In this step, BALF was added to the resulting cell suspensions which were then centrifuged at 1500 rpm for 5 min at 4°C. The supernatant was discarded, and the pellet was resuspended in Ammonium-Chloride-Potassium (ACK) lysis buffer (A1049201, Gibco), in order to lyse red blood cells, and incubated for 4 min at RT. After, PBS1x was added twice the lysis buffer volume and then centrifuged under the previously described settings. The supernatant was discarded, and the cell pellet was resuspended in PBS1x with 4% FBS (FACS) buffer. About $1x10^6$ cells from each sample were loaded onto a cytometer tube and proceeded to flow cytometry described below.

3.4. Flow cytometry

The cytometer tubes containing cell suspension from each animal were centrifuged in previously described settings. The supernatant was discarded, cell pellet was resuspended in FACS buffer containing fluorochrome-conjugated primary antibodies, indicated in Table 2, and incubated for 30min at 4°C, in the dark. After this, FACS buffer was added to the cell suspensions, which were then centrifuged, and supernatant was discarded. Cell pellets were resuspended in 100 μL of PBS containing 0.1 μL of Viable Dye (VD) eFluor® 450 (65-0863-14, EBioscience) and incubated for 30 min at 4°C, in the dark. PBS1x was then added to cell suspensions, followed by centrifugation and supernatant discard, as described above. Cell pellet was resuspended in paraformaldehyde (PFA) 4% for 20 min, followed by centrifugation and supernatant discarded, as described above. Cell pellets were resuspended in 250 μL of FACS buffer. Cells were analyzed the next day in LSR II flow cytometer system (BD Bioscience).

Table 2 - Primary antibodies and respective concentrations used in flow cytometry staining protocol.

Host specie – Reactivity Antibody	Fluorochrome Reference	Concentration
CD45 Rat anti-mouse	BV 500 103138, Biolegend	1/100
Siglec-F Rat anti-mouse	PE 552126, BD Biosciences	1/200
CD11b Rat anti-mouse	PE-Cy7 101216, Biolegend	1/100
CD64 Mouse anti-mouse	FITC 139316, Biolegend	1/200
CD11c Hamster anti-mouse	PercCP/Cy5.5 117328, Biolegend	1/100
Ly6G Rat anti-mouse	BV 605 127639, Biolegend	1/100
MHCII Mouse anti-mouse	Alexa Fluor® 647 115310, Biolegend	1/100
CD24 Rat anti-mouse	ACP-Cy7 47-0242-80, Invitrogen	1/100
CD80 Hamster anti-mouse	BV 650 104731, Biolegend	1/100
CD206 Rat anti-mouse	BV 78 141729, Biolegend	1/100

Verification of autofluorescence background and voltages were established with unstained control. Due to high number of fluorochrome used, automatic fluorescence compensation was performed using BD FACSDiva software (BD Biosciences). For this, single stained for each fluorochrome conjugated antibody was performed using AbC Total Antibody Compensation Beads Kit (A10497, Life Technologies). The gating strategy used to identify the cell populations of interest was based in Misharin el al. 2013 [64] and is demonstrated in Figure 7. Per sample were obtained 100.000 – 150.000 $CD45^+$ events. The analysis of the data acquired by BD FACSDiva software was conducted on FlowJo Software (Tree Star, Ashland, OR, USA) as outlined in Figure 7. Moreover, viable dye positivity allowed the identification of dead cells and their exclusion from the analysis, avoiding potential unspecific staining on these cells.

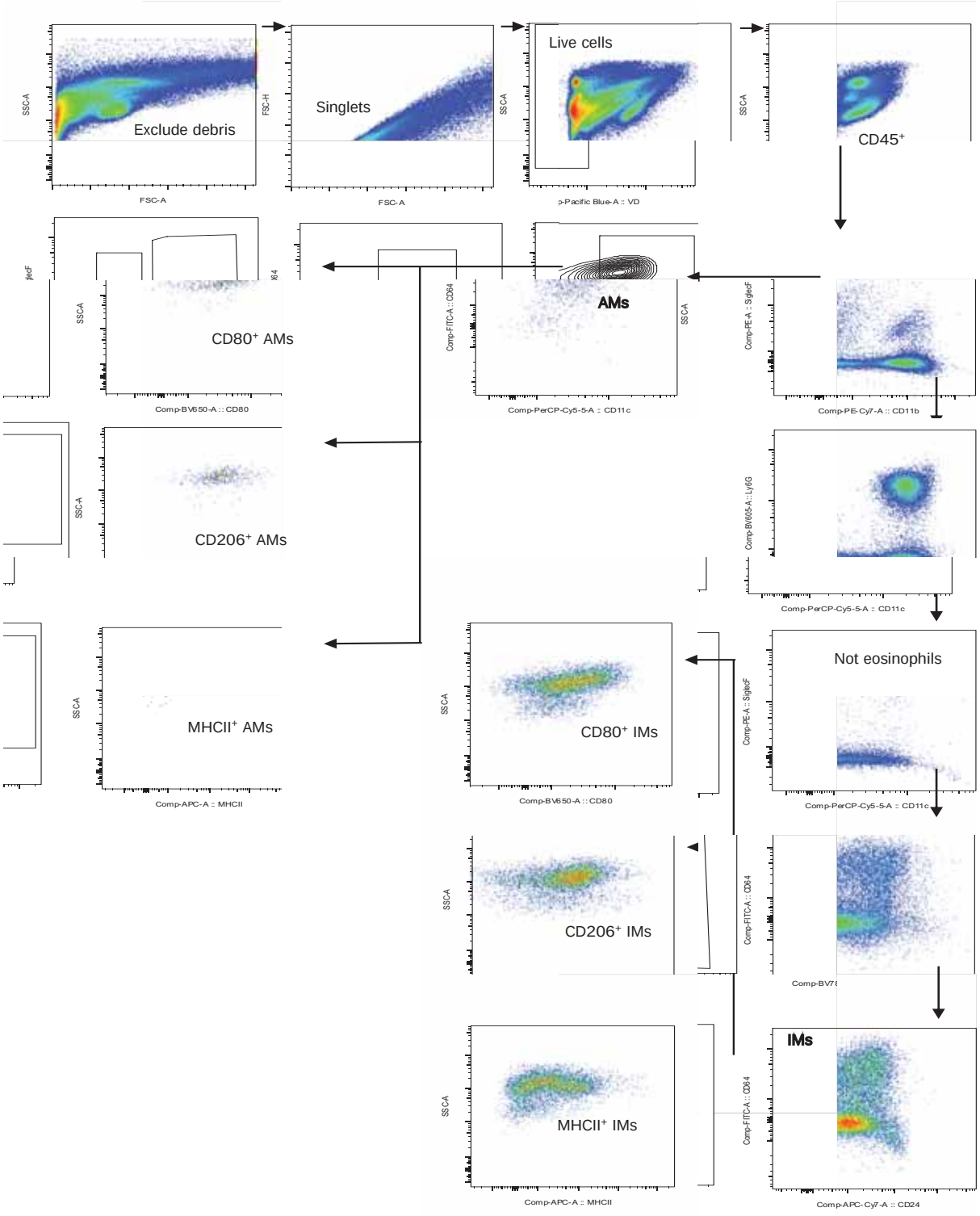


Figure 7 - Gating strategy to identify AMs and IMs at 3, 5, 7 and 9 days after BLM administration in mice.

Cells were isolated by mechanical and enzymatical dissociation of mouse lungs and stained for a mix of primary antibodie Gating for the exclusion of cell debris and doublets was achieved using side scatter vs forward (SSC-A vs FSC-A) area a forward height vs forward area (FSC-H vs FSC-A), respectively. Viable status was then interrogated to exclude dead ce followed by the identification of immune live cells by CD45 staining. The sequential gating strategy was used to identify AM (Sigle-F$^+$CD11b$^-$CD11c$^+$CD64$^+$) and to exclude immune populations like neutrophils (CD11b$^+$Ly6G$^+$) and eosinophils (Sig F$^+$CD11c$^+$), followed by the identification of IMs (CD11b$^+$MHCII$^+$CD11c$^{+/-}$CD64$^+$CD24$^-$).

3.5. Alveolar and Interstitial macrophages separation

A set of untreated animals and of 7- post BLM treatment was used to isolated MO populations by fluorescence activated cell sorting for further qRT-PCR analysis, while another set untreated, 7- and 9-days treated animals was used to obtained MO for primary culture and further collection of conditioned media. MO population obtained from untreated animals are identified as untreated AMs and untreated IMs and MO population obtained from treated animals are identified as treated AMs and treated IMs.

Following mice sacrifice via an anesthesia overdose, BALF collection and tissue dissociation were performed as described in section 3.3.

In order to enrich the populations of interest that are minor the lung, we performed CD45 immunomagnetic beads cell separation. Thus, single cell suspensions were centrifuged at 1500 rpm for 5 min at 4ºC and supernatant was discarded. Cell pellets were resuspended in 90 μL of FACS buffer per 10^7 cells followed by adding 10 μL of CD45 MicroBeads (130-052-301, Miltenyi Biotec) and incubated for 15 min at 4ºC. Cells were washed with FACS buffer, centrifuged and supernatant discarded. Then, cell pellets were resuspended in 500 μL of FACS buffer and proceeded to the magnetic separation. The MS columns (130-042-201, Miltenyi Biotec) were placed in the OctoMACS separator (130-042-109, Miltenyi Biotec) magnetic field and rinsed with 500 μL of FACS buffer. The previously magnetically labelled cell suspensions were applied onto to the columns. The liquid that first eluted from the column contained the unlabeled fractions ($CD45^-$ cells) and was discarded. Columns were washed three times with FACS buffer. After, the columns were removed from the separator and placed on a 15 mL collection tube, 1 mL of FACS buffer was pipetted onto the column and firmly apply the supplied plunger to immediately flush out the magnetically labeled $CD45^+$ cells. The obtained cell suspensions were centrifuged followed by discard of supernatant, and the cell pellet was resuspended in FACS buffer. All cells from each sample were loaded onto a cytometer tube, cells counted using trypan blue (15250061, Gibco) exclusion and proceeded to flow cytometry staining.

The cytometer tubes containing cell suspension from each animal were centrifuged in previously described settings. The supernatant was discarded, cell pellet was resuspended in FACS buffer containing fluorochrome-conjugated antibodies, indicated in Table 3, and incubated for 30 min at 4°C, in the dark. After this, FACS buffer was added to the cell suspensions, which were then centrifuged, and supernatant was discarded. Cell pellets were resuspended in 500 μL of FACS buffer and left on ice to proceed to fluorescence activated cell sorting using BD FACSARIA II cell sorter (BD Bioscience).

Table 3 - Primary antibodies and concentrations used in the flow cytometry staining protocol.

Host specie – Reactivity Antibody	Fluorochrome Reference	Concentration
CD45 Rat anti-mouse	PE-Cy7 552848, BD Biosciences	1/200
Siglec-F Rat anti-mouse	PE 552126, BD Biosciences	1/200
CD11b Rat anti-mouse	APC 553312, BD Biosciences	1/400
CD64 Mouse anti-mouse	FITC 139316, Biolegend	1/300
CD11c Hamster anti-mouse	PercCP/Cy5.5 560584, BD Biosciences	1/200
Ly6G Rat anti-mouse	APC-Cy7 560600, BD Biosciences	1/300

Verification of autofluorescence background and voltages were established with unstained control. For each fluorochrome, compensations were set using AbC Total Antibody Compensation Kit (A10497, life technologies). Due to limitations in the number of fluorochromes that could be used, a selection was made regarding the antibodies that would ensures maximal confidence in obtaining the targeted populations. Thus, cell populations were obtained by the gating strategy described in Figure 8. In each sample, 35.000 to 400.000 events were captured from the populations of interest. For qRT-PCR analysis, all cells were retrieved to tubes containing RNAprotect Cell Reagent (76526, Qiagen) and stored at -80ºC. To obtain MO conditional media, cells were recovered in 15 mL tube containing DMEM1x and proceeded to primary cell culture.

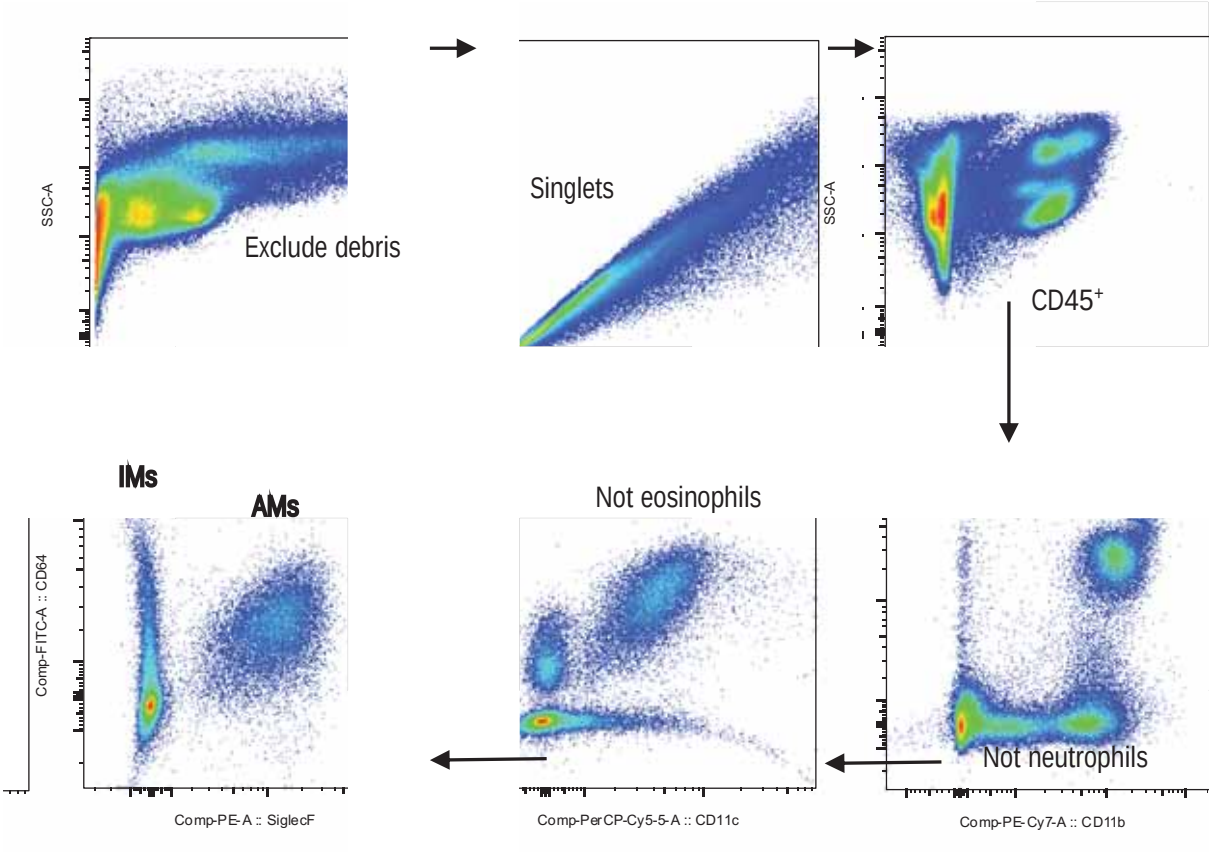


Figure 8 - Gating strategy to separate AMs and IMs at 7 and 9 days after BLM administration in mice.

Cells were isolated by mechanical and enzymatical dissociation of mouse lungs and staining for a mix of primary antibodie Gating for the exclusion of cell debris and doublets was achieved using side scatter vs forward (SSC-A vs FSC-A) area ai forward height vs forward area (FSC-H vs FSC-A), respectively. Following this, immune cells were identified by CD45 stainir The sequential gating strategy was used to exclude immune populations like neutrophils ($CD11b^{+}Ly6G^{+}$) and eosinoph ($Sigle\text{-}F^{+}CD11c^{+}$), followed by the identification of AMs ($CD11b^{+/-}CD11c^{+}CD64^{+}Sigle\text{-}F^{+}$) and IMs ($CD11b^{-}$ $CD11c^{+/-}CD64^{+}Sigle\text{-}F^{-}$).

3.6. Reverse transcriptase quantitative polymerase chain reaction

Total RNA was extracted from lung sorted MO, using RNeasy Plus Micro Kit following the instructions provided by the manufacture (74034, Qiagen). Once we obtained a limited quantity of RNA per lung of treated and untreated sorted MO, we pulled the RNA from three samples of the same condition and got a n=3 of biological samples.

Super Script III First-Strand Synthesis Supermix kit was used to convert all extracted RNA into cDNA, following the instructions provided by the manufacture (18080400, Invitrogen).

Differences in transcripts expression were analyzed by qRT-PCR. For quantitative gene expression analysis, 2 μL of cDNA were used as template and was mixed to Taqman Universal PCR MasterMix (4304437, Thermo Fisher Scientific) and one of TaqMan® Gene Expression assay indicated in Table 4.

The cycling conditions for amplification were: 10 min at 95°C, 40 cycles of 15 s at 95°C and 30 s at 60°C. Glyceraldehyde-3-phosphate dehydrogenase (*Gapdh*) gene was used as reference gene. The data was analyzed based on the ΔΔCt method [74]. Briefly, Ct values of target genes were normalized to the reference gene and the data was presented in relative transcript' expression ($2^{-\Delta Ct}$). Each measurement was conducted in duplicate.

Table 4 - TaqMan® Gene Expression assays probes used in qRT-PCR analysis.

	Gene	Reference
Reference gene	*Gapdh*	Mm99999915_g1
Pro-inflammatory genes	*Tnfa*	Mm00443258_m1
	Il-1b	Mm00434228_m1
	Ccl2	Mm01178820_m1
	Cxcl2	Mm00436450_m1
	Ccl5	Mm01302427_m1
	Ccl6	Mm01302419_m1
	Ccl9	Mm00441260_m1
Anti-inflammatory genes	*Arg1*	Mm00475988_m1
	Tgf-1b	Mm01178820_m1
	Tgbfi	Mm01337605_m1
	Chi3l3	Mm00657889_m1
	Ccl24	Mm00444701_m1
	Fn1	Mm01256744_m1
	Mmp12	Mm00500554_m1
	Retlna	Mm00445109_m1

3.7. Cell Culture

3.7.1. Primary Alveolar and Interstitial macrophages culture and collection of conditioned media

Following the collection of sorter MO, 250.000 cells were plated per well of Sterilin™ 100mm Square Petri Dishes (Thermo Fisher Scientific), in DMEM1x/10%FBS. Plates were placed at 37°C, in a humidified atmosphere containing 5% of CO_2, for 24 h. After this time, cell media which now contained the MO secreted factors, the conditioned media (CM), was collected, centrifuged at 1500 rpm for 5 min to remove any cell debris and then stored at -80°C.

3.7.2. MLg cell line

MLg cell line (MIg 2908, ATCC®CCL206™), a mouse lung fibroblasts cell line, was used in all *in vitro* assays. MLg cells were maintained in Minimum Essential Medium (MEM; 31095-029, Gibco) supplemented with 10% of FBS, 10 mM of HEPES and 1% of penicillin. Cells were maintained at 37°C in a humidified atmosphere containing 5% CO_2. When the cells reached 80-90% of confluence, they were enzymatically dissociated using TrypLE Express Enzyme (12605-028, Gibco), for 10 min at 37°C. MLg media was then added to stop the reaction and cell suspension was passed to new T-25 in a 1:25 dilution.

3.8. *In vitro* assays

3.8.1. Challenge of MLg cell line with conditioned media

MLg cells were first enzymatically dissociated as described above, followed by centrifugation at 1200 rpm for 5min. Next, supernatant was removed and cell pellet was resuspended in fresh MLg media. A small volume of cell suspension was retrieved and diluted in trypan blue to perform cell counts.
The chosen cell seeding density, explained below, was plated in MLg media and let to adhere overnight. After the adherence time, the media was removed and cells washed with PSB1x.
Five experimental conditions were tested in these assays: control condition – cell maintained in media (DMEM1x/10%FBS) used to plate sorted MO and obtain their conditioned media; Untreated AMs condition – cells stimulated with untreated AMs conditioned media; Treated AMs condition – cells stimulated with Treated AMs conditioned media; Untreated IMs condition – cells stimulated with untreated IMs conditioned media; Treated IMs condition – cells stimulated with Treated IMs conditioned media.
In the control condition wells, after the washing step, DMEM1x was added with supplementation of 10%FBS, 10 mM of HEPES and 1% of penicillin. The supplementation with FBS was necessary because we verified that when cultured without FBS MLg cells do not survive (Supplementary Fig. 1). In the wells of experimental conditions, after the washing step, the conditioned media derived from the respective primary cultured MO was added. Supplementation with 10%FBS was done to conditioned media, to maintain similar conditions to the control. Stimulation with MO-derived conditional media was performed for 48h. After this period, MLg cells were analyzed for apoptosis, metabolic activity, fibroblasts proliferative and transdifferentiation state. Regarding viability, apoptosis and metabolic activity assessment, cells were

plated in 96 well plates. For immunofluorescence assays, cells were plated in µ-Plates 96 Well Black (89626, Ibidi). Each condition was conducted in triplicates, in one independent experiment.

3.8.2. Viability curves

In order to determine the cell density to be used in all *in vitro* assays, the cell growth percentage of different concentration of plated cells was measured by Sulforhodamine B (SRB; 230162-5G, Sigma-Aldrich) assay.

MLg were plated at three concentrations of cells/well: 5000, 10000, 15000 cells/well. MLg plated in their culture media where let to adhere overnight. After this period, media was removed, cells washed with PBS1x, DMEM1x/10% FBS was added to the wells and cells were cultured for 24 h or 48 h. SRB assay was performed after the adherence period and after 24 and 48 h of culture, in order to assess the evolution of cell mass over-time. At the mentioned time-points, media was removed, and cell fixation was carried out with cold trichloroacetic acid (91228, Sigma-Aldrich) 50% (wt/vol) for 1 h, at 4°C. Cells were washed 4 times with distilled water, left to dry and after incubated with SRB solution for 30min at RT. Following this, cells were washed with acetic acid (S25118, Thermo Fisher Scientific) 1%, left to dry and Tris base 10 mM was added to the wells. At the end, absorbance at 530 nm was read using a 96-well plate reader (Varioskan® Flash - Thermo Fisher Scientific, Vantaa, Finland).

We select 5000 cells/well as the cell seeding density for the *in vitro* assays once it was the only cell seeding density in which the cells did not reach full confluence and still have space to growth upon the stimulation with MO-derived conditioned media (Supplementary Fig. 2).

3.8.3. Apoptosis assessment

Annexin V staining was performed in order to verified if the MO-derived conditioned media was inducing cell apoptosis in MLg cells. After 48 h of stimulation, media was removed, cells washed with PBS1x and then enzymatically dissociated using accutase solution (A6964-0500, Sigma- Aldrich) for 25 min at 37°C. After, cell suspension was transferred to a tube and annexin v staining was carried out using the Annexin V Apoptosis Detection Kit FITC, following the instructions provided by the manufacture (88-8005-74, eBioscience). Cells were incubated, for 5 min, with 4,6-diamidino-2-phenylindole (DAPI; Invitrogen, D1306), which allows nucleus identification. After the staining, cell suspension was transferred into coverslips and images were obtained at the inverted fluorescence microscope (Olympus widefield upright

microscope BX61, Olympus, Japan). Apoptotic cells were identified and counted by positive green staining. Data was presented as Annexin V positive cells per DAPI positive cells.

3.8.4. Immunofluorescence staining for fibroblasts proliferation and transdifferentiation

Following 48 hours of stimulation with MO-derived conditioned media, medium was carefully removed, and cells were washed with PBS1x for 5 min. All incubations and washing steps were performed in agitation and at RT. Cells fixation was carried out with PFA 4% (proliferation protocol) or Methanol 100% (transdifferentiation protocol) for 30 min. This was followed by cell permeabilization with Triton-X-100 0.3% for 20 min, in the case of the proliferation protocol. Cells were washed twice with PBS-Tween 0.5% for 10 min and blockage of non-specific binding was performed with newborn calf serum (proliferation protocol; 1/10; 186427, Biochrom) or normal goat serum (transdifferentiation protocol; 1/10; G9023-0010, Sigma-Aldrich) for 1h. Next, cells were incubated overnight with primary antibodies diluted (Table 5) in the solution of blockage of non-specific binding. Cells were washed with PBS-Tween 0.5% twice for 10 min and secondary antibodies (Table 5), diluted in the solution of blockage of non-specific binding, were added and incubated for 2 h. After this step, cells were washed with PBS-Tween 0.5% twice for 10 min and incubated with DAPI for 5min. Next, cells were washed twice with PBS1x and Ibidi Mounting Medium (50001, Ibidi) was added to the wells, in order to preserve fluorescence. For each well, three representative images were obtained at the inverted fluorescence microscope (Olympus widefield inverted microscope IX53, Olympus, Japan) using the 10x objective. Cells positive for Ki-67, Vimentin (Vim) and αSma were manually counted in the cellSens sofware (Olympus, Japan). Ki-67 positive cells were identified as cell in proliferation, Vim only positive cells were identified as fibroblasts and Vim/αSma positive cells were identified as myofibroblasts. Data was presented as % of positive cells per cell seeding density.

Table 5 - Primary and secondary antibodies used to assess fibroblast proliferation and transdifferentiation by immunofluorescence.

	Primary Antibody (Concentration; Reference)	Secondary Antibody (Concentration; Reference)
Proliferation	**Rabbit anti-mouse Ki-67** (1/250; AB9260, Millipore)	**Goat anti-rabbit 568** (1/250; a11011, Thermo Fisher Scientific)
Transdifferentiation	**Rabbit anti-mouse Vim** (1/150; #5741, CellSignalling Tech)	**Goat anti-rabbit 568** (1/250; a11011, Thermo Fisher Scientific)
	Mouse anti-mouse αSma (1/100; ab32575, Abcam)	**Goat anti-mouse 488** (1/250; a11001, Thermo Fisher Scientific)

3.8.5. Metabolic activity assessment (MTS)

Cell metabolic viability was evaluated by MTS assay (CellTiter 96 Aqueous One Solution, PROMEGA, Milan, Italy). MTS tetrazolium compound is bioreduced by metabolic viable cells into a colored formazan product that is soluble in the culture medium. After culture, conditioned media was replaced with DMEM1x/10% FBS in which was added the MTS reagent in a concentration of 1/10. The plates were incubated for 2h30 in a humidified, 5% CO2 atmosphere. Next, 490 nm absorbances were read using a 96-well plate reader (Varioskan® Flash - Thermo Fisher Scientific, Vantaa, Finland). Triplicate control wells with DMEM1x/10% FBS and without cells were used to correct the background absorbance.

3.9. Data analysis

Statistical analysis was performed in GraphPad Prism, version 6.00 (GraphPad Software, San Diego, CA). All results were expressed as group mean ± SEM (standard error of the mean). For the evaluation of flow cytometry results, a two-way ANOVA in order to compare the mean values for the three animal groups at the different time-points analyzed. Multiple comparisons between groups were accomplished through Holm-Sidak's test. For the statistical evaluation of transcript' expression levels results, differences between two groups were analyzed using Kolmogorov-Smirnov test. Values were accepted with statistically significant differences when p-value was higher than 0.05.

4. Results

4.1. Characterization of macrophage populations during the inflammation phase of BLM-induced pulmonary fibrosis mouse model

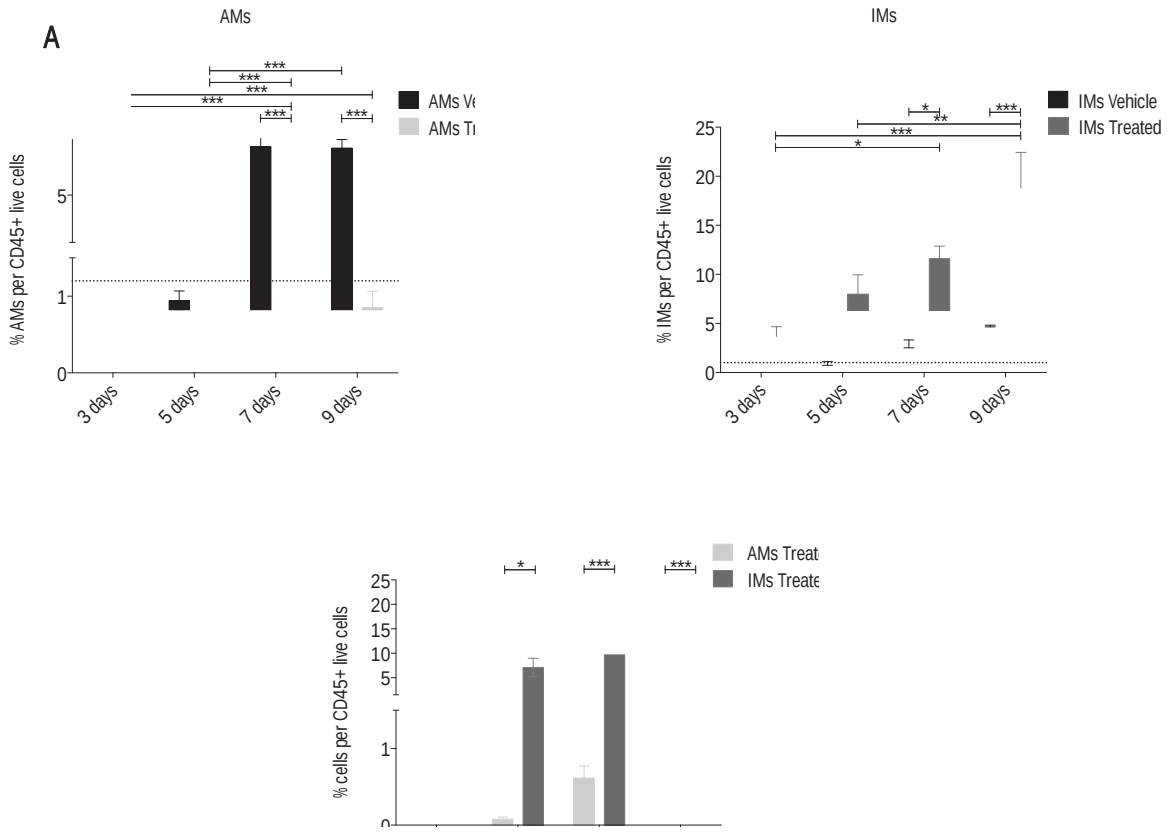
In order to understand the dynamics of lung MO populations throughout the inflammatory phase of BLM-induced pulmonary fibrosis, we analyzed, by flow cytometry, AMs and IMs at four time-points after BLM administration: 3 days (early inflammation), 5 days (progressive inflammation increase), 7days (peak of inflammatory phase), and 9days ("switch" between inflammation and fibrosis). AMs and IMs were assessed in the three experimental groups: untreated, vehicle and treated groups.

AMs and IMs were differentiated mainly by expression of cell surface marker Siglec-F, adapting a gate strategy used by Misharin et al. 2013 [64].

Regarding the AMs vehicle group, it was observed an increase of 586% at day 7 ($p < 0.0001$) and of 578% at day 9 ($p < 0.0001$), when comparing to the untreated group (Fig. 9A; Table 6). No significant differences were observed at day 3 ($p = 0.2703$) and day 5 ($p > 0.9999$) (Fig. 9A). When comparing treated and untreated AMs, it was observed that the treated group presented a tendency to decrease at day 3 ($p = 0.4134$) and day 5 ($p = 0.2840$) which is then partially restore at day 7 ($p = 0.9998$) and day 9 ($p = 0.9998$) (Fig. 9A; Table 6). Moreover, it was also verified that AMs treated group presented a decrease in all time-points assessed, when compared to the vehicle group, which did not present statistical differences at day 5 ($p = 0.9177$; Fig. 9A; Table 6).

Concerning IMs, it was found that the percentage of these cells did not change significantly, when comparing vehicle and untreated groups ($p > 0.9999$); Fig. 9B; Table 6). Moreover, IMs treated group presented an increasing tendency in all times-points assessed, when compared to vehicle groups (Fig. 9B; Table 6). This tendency was progressively higher with statistically significant differences by day 7 ($p = 0.0130$) and 9 ($p = 0.0027$), with an increase of 297% and 296%, respectively (Fig. 9B, Table 6). Similar differences were observed between treated and untreated IMs (Fig. 9B, Table 6). When comparing specifically AMs and IMs treated group clear differences were verified in representativeness of the two populations, with IMs increasing 9875% at day 5 ($p = 0.0346$), 1174% at day 7 ($p < 0.0001$) and 2109% at day 9 ($p < 0.0001$) (Fig. 9C; Table 6).

The percentages of AMs and IMs obtained in untreated and treated groups at day 7 and 9 after BLM administration through the fluorescence activated cell sorting gating strategy were also analyzed and presented similar results to the ones described here, as indicated in Supplementary Figure 3.



the inflammatory phase of BLM-induced pulmonary fibrosis.

AMs (A) were identified as CD45+Siglec-F+CD11b+/-CD64+CD11c+ and IMs (B) as CD45+CD11b+/-MHCII+CD11cCD64+CD24-, b flow cytometry, within the CD45+ population. MO cytometry analysis was performed in untreated (baseline), vehicle an treated groups. Proportion of treated AMs versus treated IMs are represented in (C). Data presented as mean±SEM (* p < 0.01; *** p < 0.001).

Group	3 days	5 days	7 day	9 days
Untreated	1.02% ± 0.20			

4.1.1. Macrophage populations activation profile

We found that after BLM administration, AMs and IMs population react differently, with a significant increase of IMs number throughout the progression of the inflammatory phase of the disease. Following this, we intended to understand how their activation profile respond to lung injury and if these populations differ also on their functionality. Thus, we first analyzed the expression of CD80, CD206 and MHCII, by flow cytometry. Macrophage pro-inflammatory phenotype is generally characterized by high expression levels of major histocompatibility complex class II (MHCII) and co-stimulatory molecule CD80, whereas CD206 high expression levels are associated with an anti-inflammatory phenotype [75,76].

Regarding CD80 positive AMs, we observe that vehicle group AMs presented a significant increase at day 7 ($p < 0.0001$) and day 9 ($p < 0.0001$) (Fig. 10A; Table 7), when compared to the control group. No differences were observed in the remaining time-points. Moreover, when comparing treated group AMs with the control, we only observed a significant increase of CD80 positive treated AMs, at day 5 ($p = 0.0433$; Fig. 10A; Table 7). CD80 positive cells were found to be significantly decrease at day 3 ($p = 0.0024$), 7 ($p < 0.0001$) and 9 ($p < 0.0001$) and significantly increase at day 5 (0.0220), when comparing treated AMs with vehicle group (Fig. 10A; Table 7). No differences were found in the percentages of CD80 positivity in treated group AMs between the day 3, 7 and 9, with the exception of day 5, in which the population was significantly higher than in the remaining days (Fig. 10A; Table 7).

Concerning CD206 positive AMs, we found a significant increase in vehicle group AMs, when comparing to the control, at day 7 ($p = 0.0008$) and day 9 ($p < 0.0001$) (Fig 10B; Table 7). No differences were observed in the other two time-points analyzed (Fig 10B; Table7). Likewise, no differences were observed in the treated AMs vs control group (Fig 10B; Table 7). When comparing CD206 positive cells on AMs from treated and vehicle groups, we found significant decrease at day 3 ($p = 0.0147$), day 7 ($p < 0.0001$) and day 9 ($p < 0.0001$) and no differences were observed at day 5 ($p = 0.8814$) (Fig 10B; Table 7). Furthermore, CD206 positive vehicle group AMs were only significantly increased at day 9, in comparation to the other analyzed time-points, and its cell positivity on treated group AMs was similar at the four days analyzed (Fig 10B; Table 7).

MHCII positive AMs of vehicle group were found to be significantly increased only at day 7 ($p < 0.0001$) and day 9 ($p < 0.0001$), when compared to the control (Fig. 10C; Table 7). No differences were found in the comparison of MHCII positive AMs of treated and control groups. Moreover, it was observed that MHCII positive cells were only significantly decrease at day 7 ($p < 0.0001$) and day 9 ($p < 0.0001$), when comparing AMs from vehicle and treated groups (Fig. 10C; Table 7). Also, MHCII positive vehicle AMs

presented a significant increase from day 5 to day 7 ($p < 0.0001$) followed by a significant decrease from day 7 to day 9 ($p < 0.0001$) (Fig. 10C; Table 7). No differences were found between days in the treated group AMs (Fig. 10C; Table 7).

Focusing on IMs profile, CD80 positive IMs, presented no differences between vehicle and control group (Fig. 10D, Table 7). Moreover, a significant increase was observed only at day 9 ($p < 0.0001$), when comparing IMs from treated and control groups, as well as treated and vehicle groups ($p < 0.0001$) (Fig. 10D, Table 7). CD80 cell positivity on vehicle group IMs was similar between the analyzed time-points, which was also verified in the treated group IMs, with the exception of the 9 day. At this day, CD80 positive treated group IMs were significantly increased (Fig. 10D, Table 7).

CD206 positive IMs presented no differences between the percentages of these cells in vehicle and control groups (Fig. 10E, Table 7). Treated versus control groups only showed significant increase on CD206 cell positivity at day 7 ($p < 0.0001$) and day 9 ($p < 0.0001$) (Fig. 10E, Table 7). Vehicle and treated CD206 positive IMs presented similar percentages, when comparing each group with the respective different time-points. At day 9, CD206 positive treated IMs were significantly increased when compared to the remaining time-points (Fig. 10E, Table 7).

Concerning MHCII positive IMs analysis, it was observed no differences between vehicle and control groups. Comparing treated and control groups percentages of MHCII positive cells, differences were found at day 7 ($p < 0.0001$) and day 9 ($p < 0.0001$) (Fig. 10F, Table 7). Treated group presented significant increase at day 7 ($p = 0.0083$) and day 9 ($p < 0.0001$) in MHCII positive IMs, when compared to the vehicle group (Fig. 10F, Table 7). No differences were found in the vehicle groups percentages, among the analyzed time-points (Fig. 10F, Table 7). MHCII positive IMs from the treated group were significantly decreased at day 5, when comparing to day 7 (< 0.0001) and day 9 (< 0.0001) (Fig. 10F, Table 7). Moreover, from day 7 to day 9 it was also observed a significant increase in MHCII positive IMs percentages from treated animals ($p = 0.0005$) (Fig. 10F, Table 7).

When relating treated AMs and IMs, it was observed that IMs presented a tendency to be increased in the majority of the time-points analyzed. Specifically, CD80 and MHCII positive cells were significantly increased at day 7($p = 0.0107$; $p < 0.0001$) and day 9 ($p < 0.0001$) (Fig. 10 G, I, Table 7) in treated IMs group. In the analysis of CD206, IMs presented significant expansion at day 5 ($p = 0.0104$), 7 ($p< 0.0001$) and 9 ($p< 0.0001$) (Fig. 10H, Table 7).

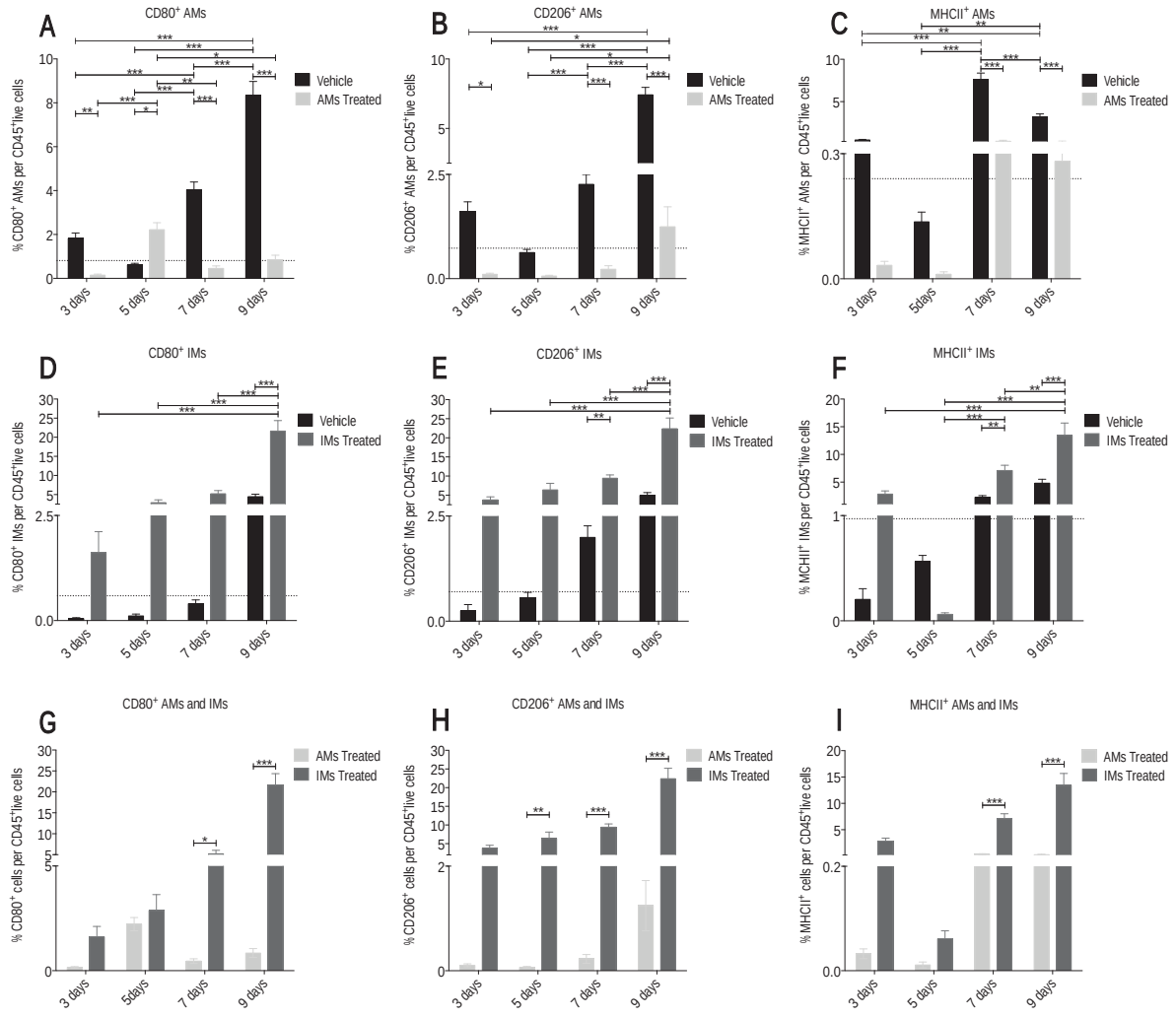


Figure 10 - Characterization of lung macrophage populations, AMs and IMs, activation profile at four time-points (3, 5, 7 9 days) of the inflammatory phase of BLM-induced pulmonary fibrosis.

CD80, CD206 and MHCII expression was analyzed in untreated, vehicle and treated AMs (A, B and C) and in untreated, vehicle-saline and treated IMs (D, E, F). Figure G, H and I display the expression of CD80, CD206 and MHCII on treated AMs versus treated IMs groups. Data presented as mean±SEM (* $p < 0.05$; ** $p < 0.01$; *** $p < 0.001$).

Table 7 - Summary of mean percentage of CD80, CD206 and MHCII positive AMs and IMs and standard error of the mean, in the animal groups tested at 4 time-points after BLM administration.

Group	Marker	3 days	5 days	7 days	9 days
AMs Untreated	CD80	0.81% ± 0.20			
	CD206	0.73% ± 0.16			
	MHCII	0.24% ± 0.07			
AMs Vehicle	CD80	2.06% ± 0.21	0.61% ± 0.05	4.04% ± 0.23	8.34% ± 0.52
	CD206	1.80% ± 0.24	0.63% ± 0.05	226% ± 0.21	7.42% ± 0.44
	MHCII	0.57% ± 0.02	0.14% ± 0.04	7.61 ± 0.66	3.17% ± 0.32
AMs Treated	CD80	0.15% ± 0.04	2.22% ± 0.27	0.46% ± 0.10	0.84% ± 0.19
	CD206	0.10% ± 0.02	0.06% ± 0.03	0.23% ± 0.09	1.25% ± 0.42
	MHCII	0.03% ± 0.00	0.01$ ± 0.00	0.34% ± 0.01	0.28% ± 0.06
IMs Untreated	CD80	0.59% ± 0.14			
	CD206	0.70% ± 0.15			
	MHCII	0.97% ± 0.18			
IMs Vehicle	CD80	0.05% ± 0.02	0.11% ± 0.03	0.40% ± 0.08	4.46% ± 0.53
	CD206	0.25% ± 0.11	0.55% ± 0.10	1.99% ±0.24	4.93% ± 0.62
	MHCII	0.20% ± 0.08	0.56% ± 0.04	2.28% ± 0.25	4.18% ± 0.58
IMs Treated	CD80	1.62% ± 0.41	2.87% ± 0.62	5.22% ± 0.75	21.61% ± 2.38
	CD206	3.78% ± 0.64	6.38% ± 1.46	8.83% ± 0.87	22.40% ± 2.43
	MHCII	2.83% ± 0.48	0.06% ± 0.01	7.11% ± 0.83	13.44% ± 1.88

Inflammatory mediators are clearly involved in the progression of fibrosis. In other to dissect if the expression of activation profile is changed in lung macrophages populations at the inflammatory phase of BLM-induced pulmonary fibrosis, we determined the expression levels of several pro-inflammatory genes (*Tnfa, Il-1b,* CC chemokine ligand *(Ccl) 2,* CXC chemokine ligand *(Cxcl) 2, Ccl5, Ccl6 and Ccl9*) as well as anti-inflammatory genes (Arginase (*Arg)1, Tgf-1b, Tgfbi,* Chitinase-like 3 *(Chi3l3), Ccl24, Fn1, Mmp12,* Resistin like alpha *(Retnla)*). The selection of assessed genes was based on a study from McCubbrey. et al 2018 [77], that performed a RNA-seq analysis of AMs and IMs populations at 8 days after BLM administration. From this study we selected genes significant altered expression in the treated IMs population.

Overall, we found no significant statistically significant differences in the analyzed gene expressions (Fig. 11). However, several trends were unquestionable.

Regarding the expression of pro-inflammatory genes, it was found that treated group AMs presented increase of 889% in *Il-1b* (Fig. 11B, Table 8), 707% in *Ccl2* (Fig. 11C, Table 8), 2900% in *Ccl5* (Fig. 11E, Table 8) and 369% in *Ccl9* (Fig. 11F, Table 8) expression, when compared to untreated group AMs. In

the comparison of the two treated group MO populations, it was observed that IMs presented increase of 370% in *Ccl2* (Fig. 11C, Table 8) and 355% in *Ccl9* (Fig. 11F, Table 8) expression and decrease of 53% in *Ccl6* (Fig. 11F, Table 8) and 68% in *Ccl5* (Fig. 11E, Table 8) expression, when compared to AMs.

Concerning the expression of anti-inflammatory genes, it was observed that treated group AMs presented an increase of 12000% in *Arg1* (Fig. 11H, Table 8) and of 490% in *Mmp12* (Fig. 11N, Table 8) expression, when compared with untreated AMs. It was verified that treated group IMs presented an increase of 383% in *Arg1* (Fig. 11H, Table 8), of 214% in *Chi3l3* (Fig. 11K, Table 8) and of 156% in *Ccl24* (Fig. 11L, Table 8) expression, and decrease of 68% in *Tgf-1b* (Fig. 11J, Table 8),and 96% in *Retnla* (Fig. 11O, Table 8) expression, when compared to untreated group IMs.

Regarding the treated groups, it was observed an increase of 695% in *Arg1* (Fig. 11H, Table 8), 123% in *Tgfbi* (Fig. 11J, Table 8), 859% in *Ccl24* (Fig. 11L, Table 8), 178% in *Fn1* (Fig. 11M, Table 8), 1209% in *Mmp12* (Fig. 11N, Table 8) and 441% in *Retnla* (Fig. 11O, Table 8) expression in IMs. On the other hand, decrease expression of 40% in *Tgf-1b* (Fig. 11I, Table 8) and 90% in *Chi3l3* was observed (Fig. 11K, Table 8).

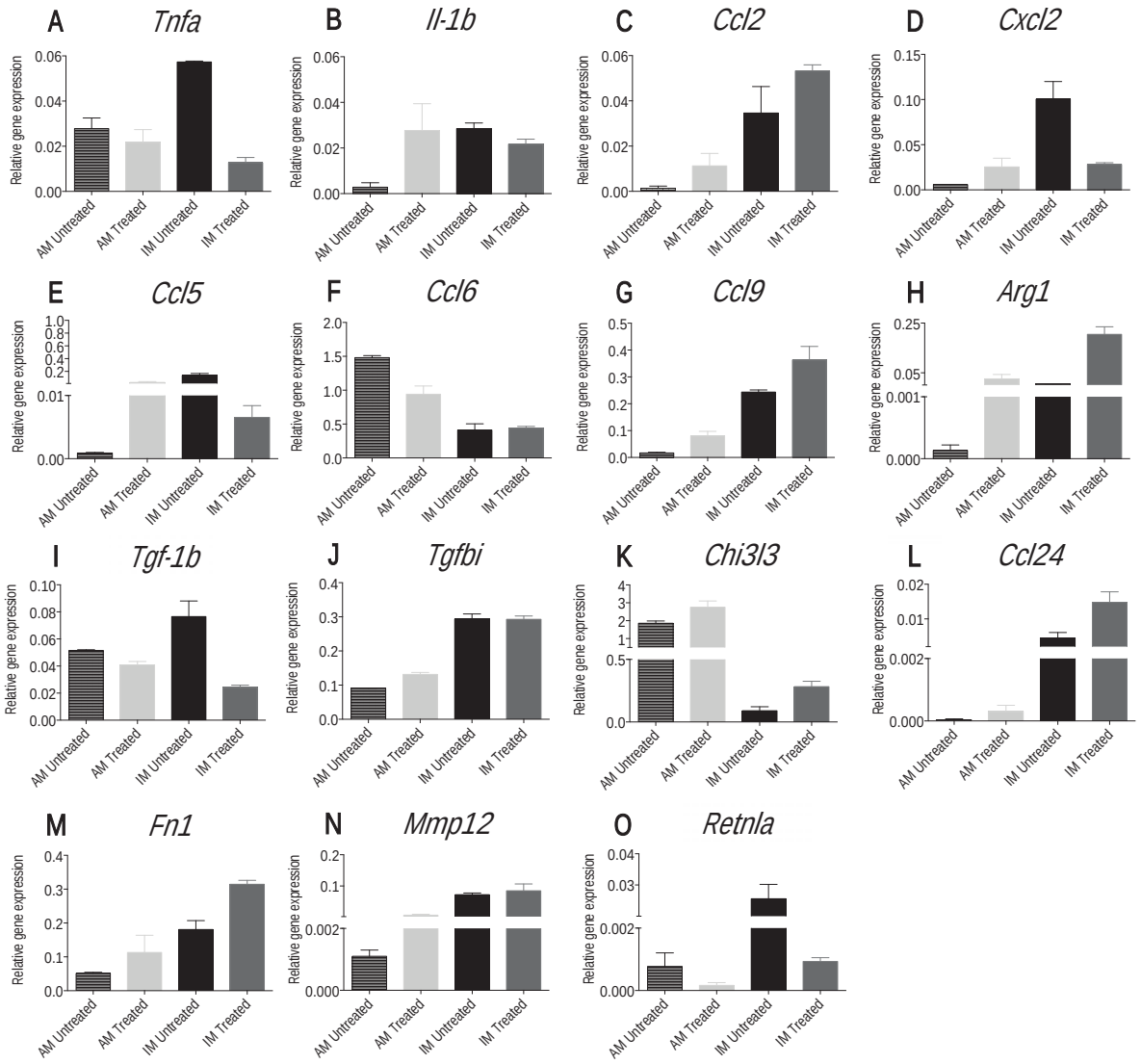


Figure 11 - Transcript' expression analysis of pro- and anti-inflammatory mediators at day 7 after BLM administration.

Pro-inflammatory namely, *Tnfa* (A), *Il-1b* (B), *Ccl2* (C), *Cxcl2* (D), *Ccl5* (E), *Ccl6* (F) and *Ccl9* (G) and anti-inflammatory namely *Arg1* (H), *Tgf-1b* (I), *Tgfbi* (J), *Chi3l3* (K), *Ccl24* (L), *Fn1* (M), *Mmp12* (N), *Retnla* (O) transcript' levels were analyzed in total RNA obtained of sorted AMs and IMs from treated and untreated mice lung, by qRT-PCR.

Expression levels were normalized to Gapdh. Data presented as mean±SEM.

Table 8 - Summary of gene relative expression levels mean and standard error of the mean in sorted AMs and IMs from untreated and treated animals groups.

GENES	AMs Untreated	AMs Treated	IMs Untreated	IMs Treated
Tnfa	0.0278 ± 0.0047	0.0217 ± 0.0057	0.0573 ± 0.004	0.0127 ± 0.0023
il-1b	0.0028 ± 0.0019	0.0277 ± 0.0117	0.0285 ± 0.0025	0.0216 ± 0.0022
Ccl2	0.0014 ± 0.0010	0.0113 ± 0.0055	0.0346 ± 0.0117	0.0532 ± 0.0027
Cxcl2	0.0057 ± 0.0004	0.0254 ± 0.0097	0.1005 ±0.0194	0.0281 ± 0.0019
Ccl5	0.0009 ± 0.0001	0.0277 ± 0.0117	0.1367 ± 0.0316	0.0086 ± 0.0023
Ccl6	1.4807 ± 0.0295	0.9406 ± 0.1215	0.4103 ± 0.0946	0.4368 ± 0.0287
Ccl9	0.0170 ± 0.0023	0.0798 ± 0.0177	0.2436 ± 0.0080	0.3629 ± 0.0507
Arg1	0.0002 ± 0.0001	0.0257 ± 0.0177	0.0052 ± 0.0005	0.2042 ± 0.0307
Tgb-1b	0.0515 ± 0.0005	0.0407 ± 0.0027	0.0766 ± 0.0115	0.0242 ± 0.0017
Tgfbi	0.0907 ± 0.0004	0.1313 ± 0.0060	0.2934 ± 0.0153	0.2928 ± 0.0098
Chi3l3	1.8555 ± 0.1322	2.7609 ± 0.3387	0.0900 ± 0.0321	0.2823 ± 0.0432
Ccl24	0.0000 ± 0.000	0.0012 ± 0.0009	0.0044 ± 0.0017	0.0113 ± 0.0038
Fn1	0.0512 ± 0.0034	0.1133 ± 0.0506	0.1808 ± 0.0263	0.3145 ± 0.0116
Mmp12	0.0011 ± 0.0002	0.0065 ± 0.0030	0.0722 ± 0.0055	0.0849 ± 0.0217
Retlna	0.0007 ± 0.0004	0.0002 ± 0.0001	0.0256 ± 0.0046	0.0009 ± 0.0001

4.2. Paracrine abilities of lung macrophage populations on fibroblast proliferation and transdifferentiation

In order to address the effects of MO conditioned media in fibroblasts characteristics, we performed *in-vitro* assays in which mouse lung fibroblasts cell line were stimulated with AMs- and IMs-derived conditioned media. Conditioned media was obtained from separated lung MO populations primary culture at 7 and 9 days after BLM administration. After stimulation, we verified whether the conditioned media was inducing cell apoptosis by immunofluorescence, in which annexin V positive cells were quantified. Cells proliferation state was also assessed by immunofluorescence, in which quantification of Ki-67 positive cells was performed. Moreover, metabolic activity of these cells was also assessed, by MTS assay. Then and also using immunofluorescence technique, fibroblasts transdifferentiation state was evaluated by the quantification of αSma and Vim positive cells (myofibroblasts) and Vim only positive cells (fibroblasts).

4.2.1. Alveolar and Interstitial macrophages-derived conditioned media of 7 days after BLM administration

After 48 hours of stimulation with MO-derived conditioned media, cell confluency and morphology were observed (Fig. 12). Untreated IMs conditions presented the lowest observed cell confluency (20%) (Fig. 12D). The control and untreated AMs conditions showed similar levels of cell confluency (50-60%), which appeared to be lower than the remaining conditions (Fig. 12A, B). Treated AMs and IMs sorted conditions presented similar cell confluency (80-90%) (Fig. 12C, E). The majority of the cells in these conditions presented increased cytoplasm and spindle-shaped morphology.

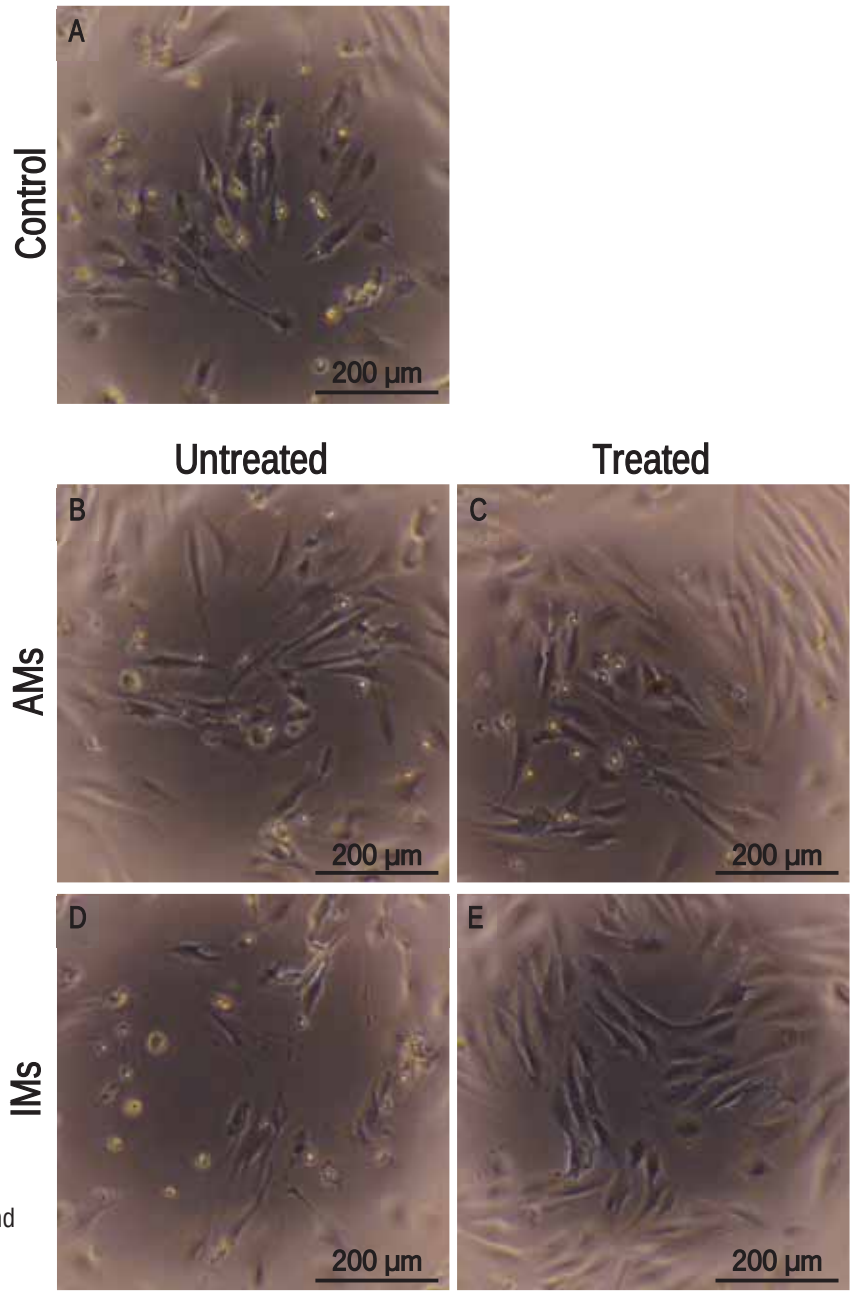


Figure 12, legend on next page

Figure 12 - Representative images of cell confluency and morphology observation in brightfield microscopy of mouse lung fibroblasts cell line after 48h stimulation with lung MO-derived conditioned media.

Lung mouse fibroblasts cell line were plated (5000 cells per well) and let to adhere for 18h hours and afterwards stimulated for 48h hours. As control condition (A) fibroblasts were maintained in their normal culture media. Conditioned media from primary culture of AMs sorted from untreated (B) and treated (C) mouse lungs and of IMs sorted from untreated (D) and treated (E) mouse lungs.

The analysis of Annexin V positive cells showed that treated AMs conditioned media was the only condition that induced apoptosis, with 25% of the cells staining for annexin V (Table 9). All the other conditions did not induce positivity for Annexin V and there for were not inducing apoptosis (Table 9).

Table 9 - Quantification of Annexin V positive cells per DAPI positive cells of mouse lung fibroblasts, after 48h stimulation with lung MO conditioned media.

	Annexin V$^+$cells/DAPI$^+$ cells
Control	0 / 4
AMs Untreated	0 / 6
AMs Treated	1 / 4
IMs Untreated	0 / 4
IMs Treated	0 / 6

Regarding fibroblasts proliferative state, no differences were observed in untreated AMs and IMs conditioned media, when comparing to the control (Fig. 13F; Table 10). It was verified a trend to increase Ki-67 positive cells in the treated AMs and IMs conditions, when comparing to the control (Fig. 13F; Table 10). This tendency appears to be similar between treated AMs and IMs conditions (Fig. 13F; Table 10). While no differences were observed regarding untreated versus treated AMs-derived conditioned media (Fig. 13F; Table 10), a tendency to increase Ki-67 positive cells was observed in the treated IMs condition, when compared to untreated IMs condition (Fig. 13F; Table 10).

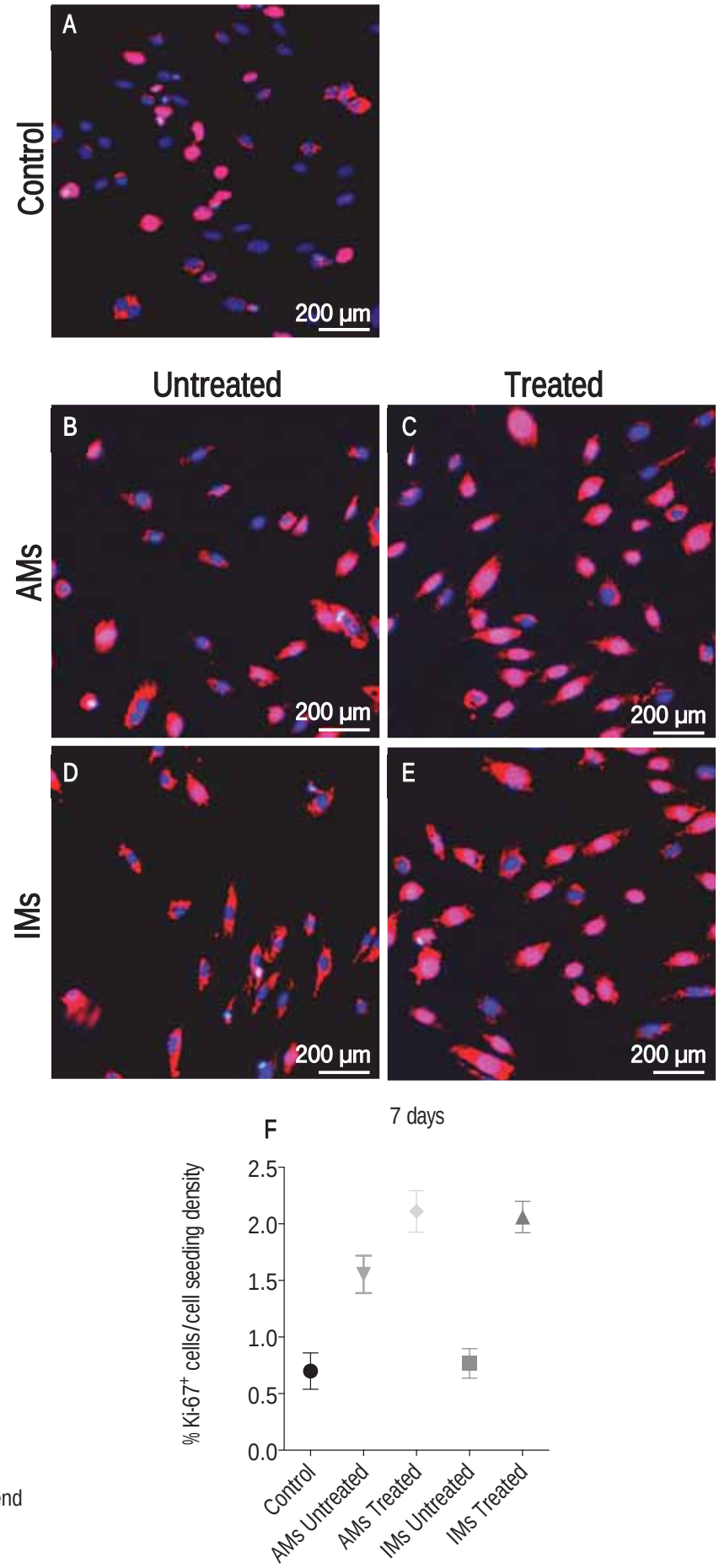


Figure 13, legend on next page

Figure 13 - Assessment of fibroblast proliferative state after 48 hours of stimulation with lung MO-derived conditioned media.
Representative images of Ki-67 immunofluorescence to identify proliferative cells (A-E). As control condition (A) a lung mouse fibroblasts cell line was maintained in their normal culture media. Fibroblasts were stimulated with conditioned media from primary culture of AMs sorted from untreated (B) and treated (C) mouse lungs and IMs sorted from untreated (D) and treated (E) mouse lungs. Graphical representation of Ki-67 positive cells quantification (F). Images were acquired with a 10x objective. Blue staining corresponds to DAPI positive cells. Data presented as mean±SEM of three technical replicates.

Table 10 - Summary of Ki-67 positive cells percentages mean and standard error of the mean in the tested conditions.

Marker	Control	AMs Untreated	AMs Treated	IMs Untreated	IMs Treated
Ki-67+	0.700% ± 0.160	1.553% ± 0.165	2.110% ± 0.183	0.767% ±0.131	2.060% ± 0.138

The metabolic activity assessment showed no differences between the tested conditions (Fig. 14, Table 11). However, treated AMs- and IMs-derived conditioned media conditions presented a tendency to have higher metabolic activity, when compared to the control and respective untreated conditions (Fig. 14, Table 11).

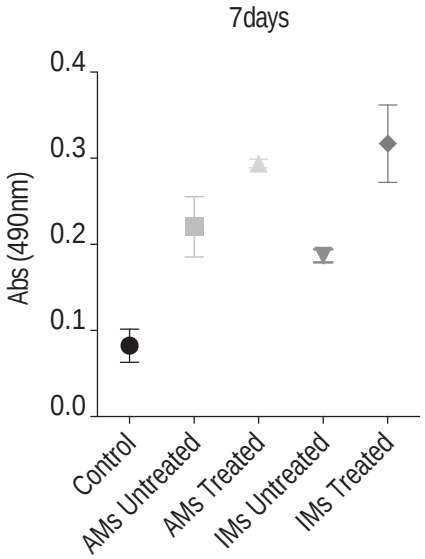


Figure 14 - Assessment of metabolic viability of adherent cells, after 48 hours of stimulation with sorter lung MO-derived conditioned media.
Cell metabolic viability was measure after the stimulation of mouse lung fibroblasts cell line with conditioned media of primary culture from sorted untreated and treated AMs and IMs (A), by MTS assay. Cells were incubated with MTS reagent for 2h30 and after absorbances (490nm) were recorded. Fibroblast normal culture media wells with no cells were used as control condition to correct the background absorbance. Data presented as mean±SEM of three technical replicates.

Table 11 - Summary of absorbance levels mean and standard error of the mean in the tested conditions.

MTS	Control	AMs Untreated	AMs Treated	IMs Untreated	IMs Treated
abs(490nm)	0.082 ± 0.019	0.220 ± 0.035	0.294 ± 0.005	0.187 ± 0.008	0.317 ± 0.045

By assessing fibroblast transdifferentiation state, we observed that all tested conditions presented a trend of lower percentages of Vim positive cells when compared to the control (Fig. 15P; Table 12). Furthermore, we observed a tendency to increase αSma and Vim positive cells in all conditions when comparing with the control, with the treated IMs-derived conditioned media condition presenting the highest percentage of αSma and Vim positive cells (Fig. 15Q; Table 12). No differences were seen in αSma and Vim positive cells when comparing untreated and treated AMs conditions (Fig. 15Q; Table 12). However, when comparing untreated and treated IMs conditions, a clear increase trend of αSma and Vim positive cells was observed in the treated condition (Fig. 15Q; Table 12).

The condition that induced the highest levels of mature myofibroblasts development was the treated IMs-derived conditioned media condition, which presented a rising trend of αSma and Vim positive cells, comparatively to the treated AMs conditions (Fig. 15R; Table 12). Treated IMs-derived conditioned media condition presented also a tendency to higher percentages of Vim positive cells, when compared with treated AMs-derived conditioned media condition (Fig. 15R, Table 12).

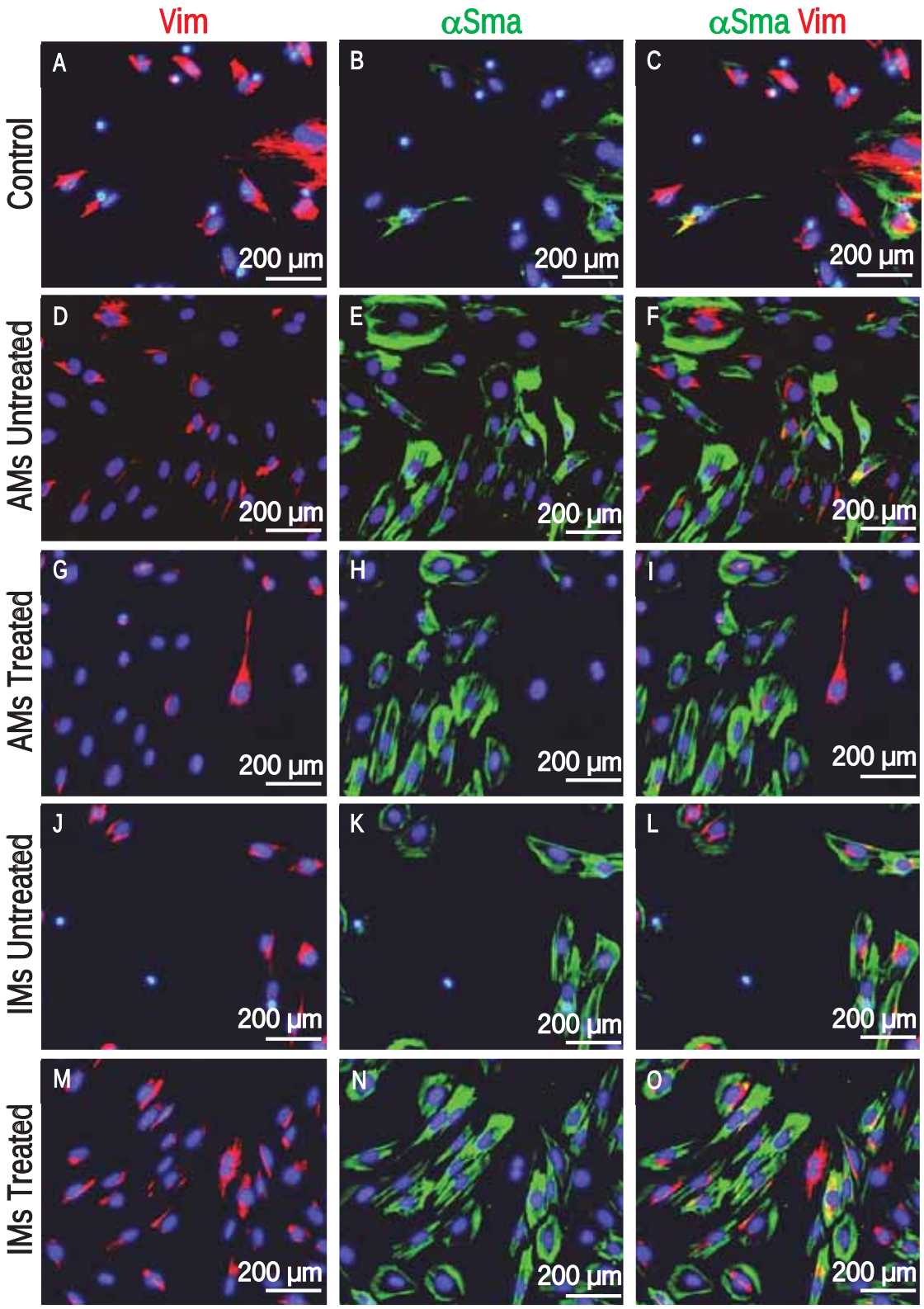


Figure 15 continues on the next page; legend on next page

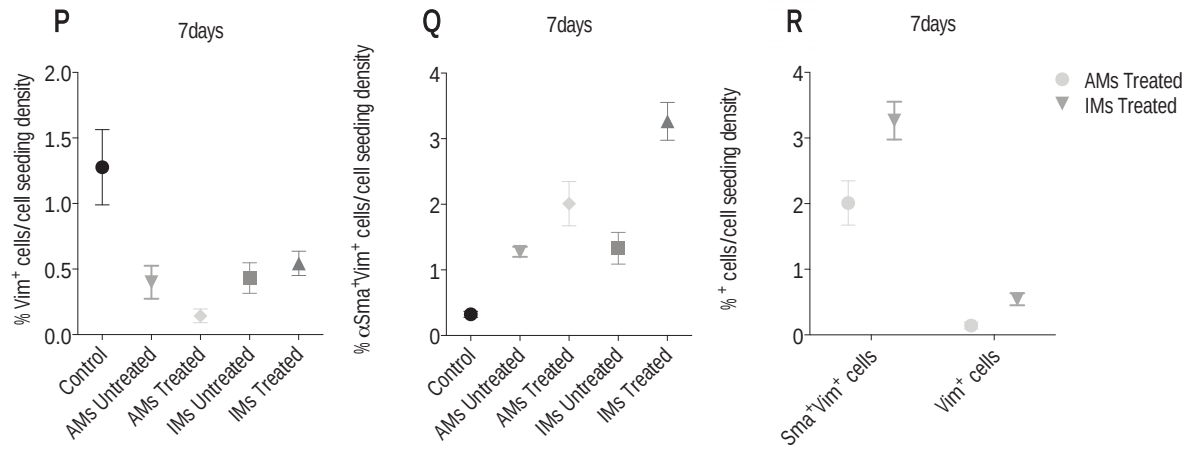


Figure 15 - Assessment of fibroblast transdifferentiation state after 48 hours of stimulation with lung MO-derived conditioned media.

Representative images of Vim, αSma and DAPI immunofluorescence to identify fibroblasts (Vim only positive cells; Fig. A, D, G, J, M) and mature myofibroblasts (αSma and Vim positive cells; Fig. C, F, I, L, O). As control condition (A, B, C) a lung mouse fibroblasts cell line was maintained in normal culture media. Fibroblasts were stimulated with conditioned media from primary culture of AMs sorted from untreated (D, E, F) and treated (G, H, I) mouse lungs and IMs sorted from untreated (J, K, L) and treated (M, N, O) mouse lungs. Graphical representation of the quantification of Vim positive cells (fibroblasts; (P)), αSma positive cells (Q) and αSma and Vim positive cells (mature myofibroblasts, (R)). Images were acquired with a 10x objective. Blue staining corresponds to DAPI positive cells. Data presented as mean±SEM of three technical replicates.

Table 12 - Summary of Vim and αSma/Vim positive cells percentages mean and standard error of the mean in the tested conditions.

Marker	Control	AMs Untreated	AMs Treated	IMs Untreated	IMs Treated
Vim+	1.277% ± 0.287	0.400% ± 0.126	0.143% ± 0.053	0.432% ± 0.117	0.543% ± 0.092
αSma+ Vim+	0.324% ± 0.004	1.276% ± 0.078	2.010% ± 0.337	1.347% ± 0.249	3.360% ± 0.092

4.2.2. Alveolar and Interstitial macrophages-derived conditioned media of 9 days after BLM administration

As well as in the 7 days conditional media assay, at day 9 after BLM administration we separated AMs and IMs from treated and untreated animals, cultured them, collected their conditioned media and stimulated lung mouse fibroblasts with this conditioned media. It was observed that, after 48 hours of stimulation, cell confluency and morphology were similar between control and untreated IMs conditions (confluency 50-60%) (Fig. 16A, D). Untreated and treated AMs conditions presented lower cell confluency

(20-30%) accompanied by increased cellular debris in suspension, when compared to the other conditions (Fig. 16B, C). Moreover, treated IMs conditioned media condition appeared to have the highest cell confluency (80-90%) (Fig. 16E). However, the majority of the cells in this condition do not present increased cytoplasm and spindle-shaped morphology.

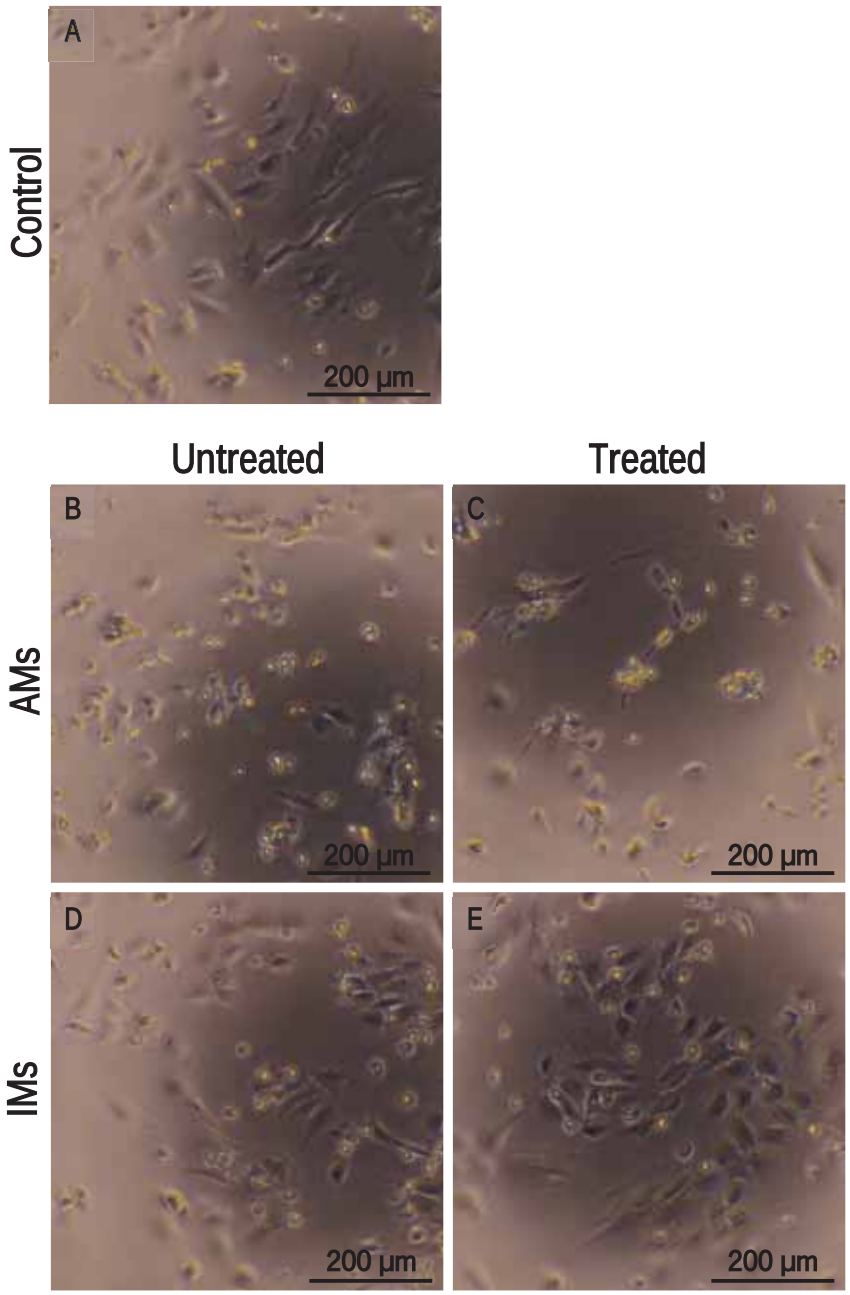


Figure 16 - Representative images of cell confluency and morphology observation in brightfield microscopy of mouse lung fibroblasts cell line after 48h stimulation with lung MO-derived conditioned media.

Lung mouse fibroblasts cell line were plated (5000 cells per well) and let to adhere for 18h hours and afterwards stimulated for 48h hours. As control condition (A) fibroblasts were maintained in their normal culture media. Conditioned media from primary culture of AMs sorted from untreated (B) and treated (C) mouse lungs and of IMs sorted from untreated (D) and treated (E) mouse lungs.

The apoptosis evaluation showed that treated AMs- and IMs-derived conditioned media conditions induced apoptosis, with 25% and 9%, of the cells staining for Annexin V, respectively (Table 13). The other conditions did not present cells staining positive for Annexin V (Table 13).

Table 13 - Quantification of Annexin V positive cells per DAPI positive cells of mouse lung fibroblasts cell line, after 48h stimulation with lung MO-derived conditioned media.

	Annexin V^+ cells/$DAPI^+$ cells
Control	0 / 4
AMs Untreated	0 / 5
AMs Treated	1 / 4
IMs Untreated	0 / 3
IMs Treated	1 / 11

Fibroblast proliferative state assessment showed untreated AMs- and IMs-derived conditioned media conditions with no significant changes in percentages of Ki-67 positive cells, when compared with control (Fig. 17F, Table 14). Also comparing to the control condition, treated AMs-derived conditioned media presented a trend to decrease Ki-67 positive cells, while treated IMs- derived conditioned media condition presented a tendency to increase Ki-67 positive cells (Fig. 17F, Table 14). This increase indicates a augment in proliferative state induced by treated IMs-derived conditioned media (Fig. 17F, Table 14). While no differences were observed in untreated versus treated IMs conditions (Fig. 17F; Table 14), a decreasing trend of Ki-67 positive cells was observed in the treated AMs-derived conditioned media, when compared to the respective untreated situation (Fig. 17F; Table 14). Regarding the treated conditions, IMs-derived conditioned media induced higher levels of Ki-67 positive cells than AMs-derived conditioned media (Fig. 17F; Table 14).

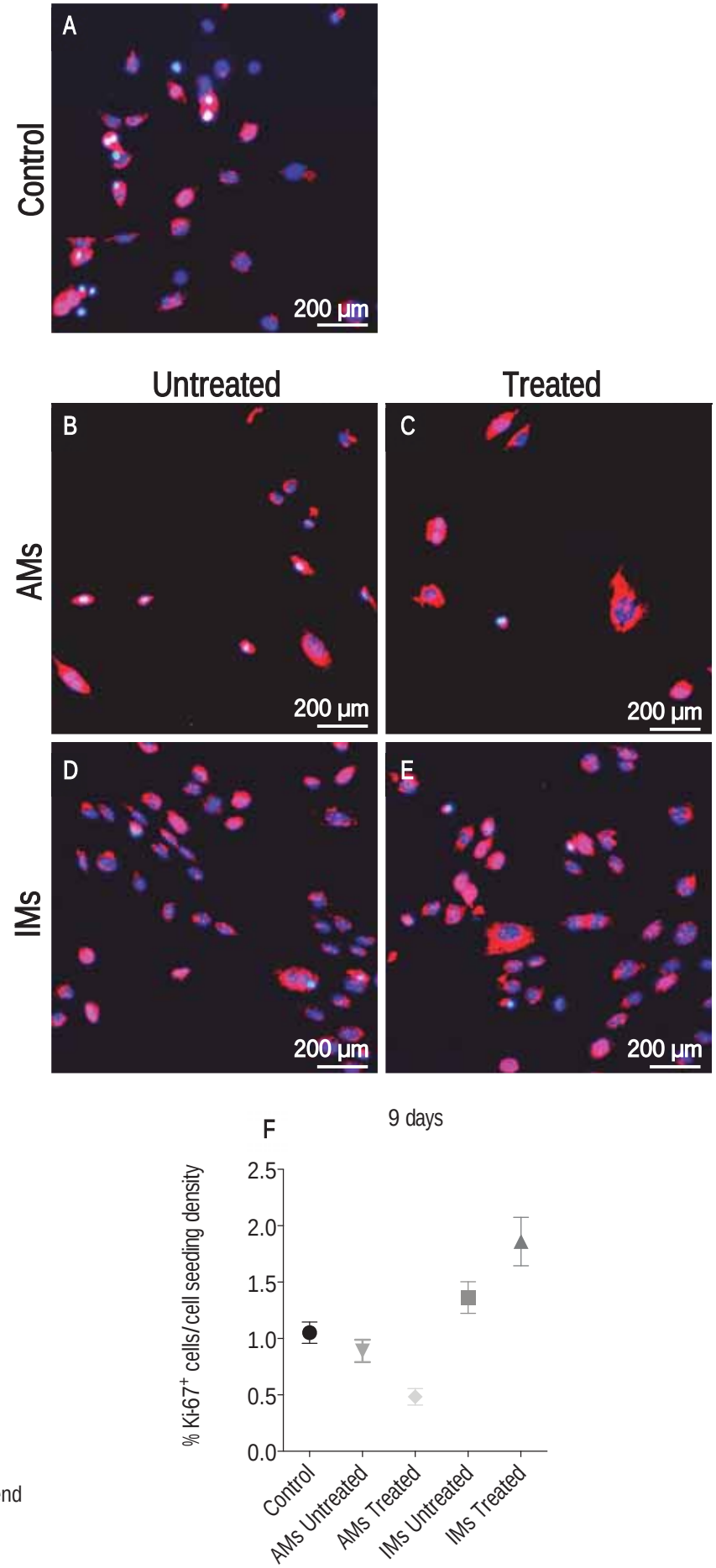


Figure 17, legend on next page

Figure 17 - Assessment of fibroblast proliferative state after 48 hours of stimulation with lung MO-derived conditioned media.
Representative images of Ki-67 immunofluorescence to identify proliferative cells (A-E). As control condition (A) a lung mouse fibroblasts cell line was maintained in their normal culture media. Fibroblasts were stimulated with conditioned media from primary culture of AMs sorted from untreated (B) and treated (C) mouse lungs and IMs sorted from untreated (D) and treated (E) mouse lungs. Graphical representation of Ki-67 positive cells quantification (F). Images were acquired with a 10x objective. Blue staining corresponds to DAPI positive cells. Data presented as mean±SEM of three technical replicates.

Table 14 - Summary of Ki-67 positive cells percentages mean and standard error of the mean in the tested conditions.

Marker	Control	AMs Untreated	AMs Treated	IMs Untreated	IMs Treated
Ki-67$^+$	1.052% ± 0.094	0.890% ± 0.010	0.483% ± 0.073	1.363% ± 0.140	1.860% ± 0.215

Regarding cellular metabolic activity, no differences were found between conditions (Fig. 18). However, untreated and treated AMs-derived conditioned media conditions presented a tendency of lower cellular metabolic activity and untreated IMs to higher metabolic activity (Fig. 18A, Table 15).

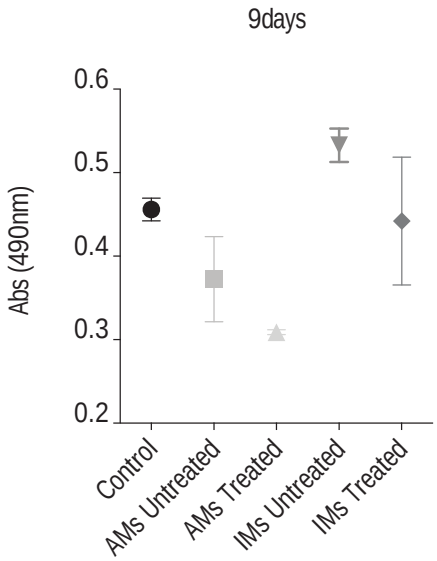


Figure 18 - Assessment of metabolic viability of adherent cells, after 48 hours of stimulation with sorter lung MO-derived conditioned media.
Cell metabolic viability was measure after the stimulation of mouse lung fibroblasts cell line with conditioned media of primary culture from sorted untreated and treated AMs and IMs (A), by MTS assay. Cells were incubated with MTS reagent for 2h30 and after absorbances (490nm) were recorded. Fibroblast normal culture media wells with no cells were used as control condition to correct the background absorbance. Data presented as mean±SEM of three technical replicates.

Table 15 - Summary of absorbance levels mean and standard error of the mean in the tested conditions.

MTS	Control	AMs Untreated	AMs Treated	IMs Untreated	IM Treated
abs(490nm)	0.456 ± 0.014	0.372 ± 0.019	0.309 ± 0.003	0.533 ± 0.020	0.442 ± 0.076

Regarding fibroblast transdifferentiation state, we found no differences in Vim only positive cells, when comparing to all conditions the control as well as treated versus untreated AMs-derived conditioned media conditions (Fig. 19P, Table 16). However, treated IMs-derived conditioned media condition presented a trend of higher levels of Vim only positive cells than untreated IMs condition (Fig. 19P, Table 16). Regarding αSma and Vim positive cells, untreated and treated AMs-derived conditioned media conditions presented similar percentages when compared to the control condition (Fig. 19Q; Table 16). Also in comparison to the control, an increase tendency of αSma and Vim positive cells was observed in fibroblasts stimulated with untreated and treated IMs-derived conditioned media (Fig. 19Q; Table 16). No differences were observed in untreated versus treated AMs and untreated versus treated IMs conditions (Fig. 19Q; Table 16). The conditioned media retrieved from treated AMs at 9 days after BLM administration do not appear to induce mature myofibroblasts formation, as the percentage of αSma and Vim positive cells is residual (Fig. 19R; Table 16). Interestingly, in the treated IMs-derived conditioned media condition, the percentage of αSma and Vim positive cells and Vim only positive cells are both showing an increased trend, when compared to the treated AMs (Fig. 19R, Table 16).

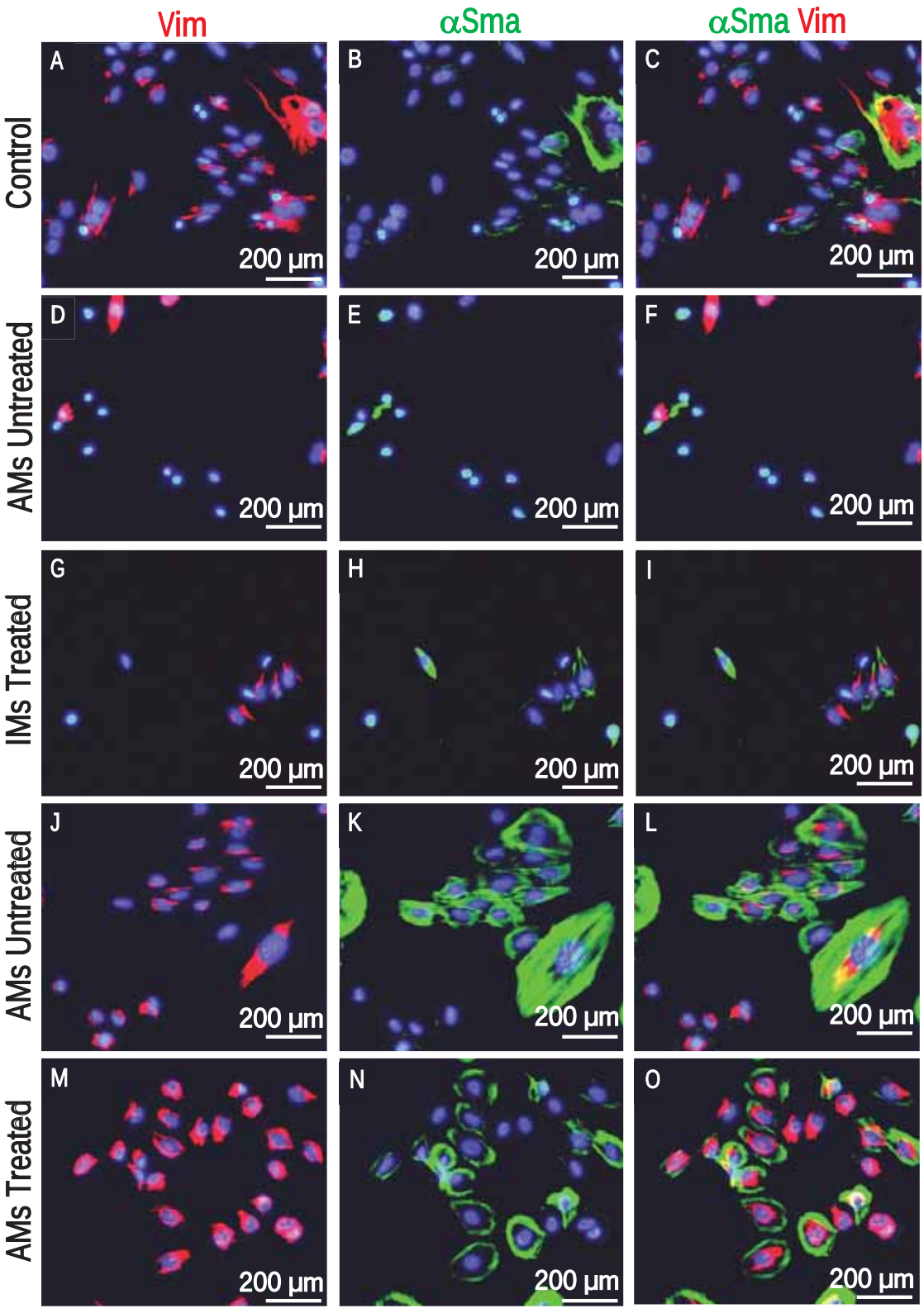


Figure 19 continues on the next page; legend on next page

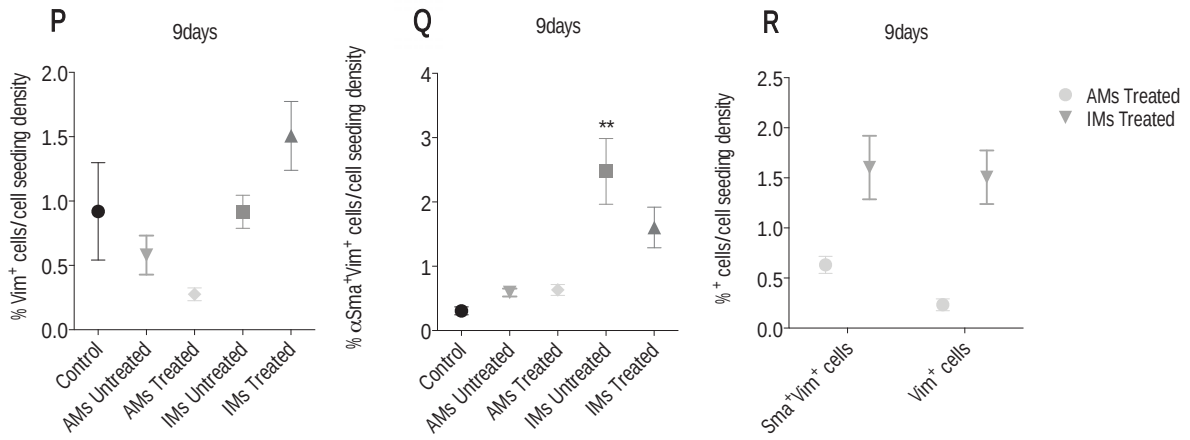


Figure 19 - Assessment of fibroblast transdifferentiation state after 48 hours of stimulation with lung MO-derived conditioned media.

Representative images of Vim, αSma and DAPI immunofluorescence to identify fibroblasts (Vim only positive cells; Fig. A, D, G, J, M) and mature myofibroblasts (αSma and Vim positive cells; Fig. C, F, I, L, O). As control condition (A, B, C) a lung mouse fibroblasts cell line was maintained in normal culture media. Fibroblasts were stimulated with conditioned media from primary culture of AMs sorted from untreated (D, E, F) and treated (G, H, I) mouse lungs and IMs sorted from untreated (J, K, L) and treated (M, N, O) mouse lungs. Graphical representation of the quantification of Vim positive cells (fibroblasts; (P)), αSma positive cells (Q) and αSma and Vim positive cells (mature myofibroblasts, (R)). Images were acquired with a 10x objective. Blue staining corresponds to DAPI positive cells. Data presented as mean±SEM of three technical replicates.

Table 16 - Summary of Vim and αSma/Vim positive cells percentages mean and standard error of the mean in the tested conditions.

Marker	Control	AMs Untreated	AMs Treated	IMs Untreated	IMs Treated
Vim+	0.920% ± 0.378	0.580% ± 0.152	0.276% ± 0.050	0.917% ± 0.128	1.501% ± 0.267
αSma+ Vim+	0.306% ± 0.061	0.592% ± 0.061	0.632% ± 0.085	2.476% ± 0.511	1.603% ± 0.317

5. Discussion

IPF is a chronic fibrosing interstitial lung disease of unknown etiology in which patients present a poor prognosis. The majority of potential treatments for disease were either completely ineffective, or, only able to slow the decline of lung function, like pirfenidone and nintedanib. However, neither of these drugs has been shown to reduced symptoms or improve patient quality of life [78]. The inefficacy of these treatments is probably due to a incomplete understanding of IPF initiation and progression. Consequently, there is an increased bet and interest in studies from more basic biological fields. This is allowing new insights in key molecular and cellular mechanisms that are modulating the disease, allowing the understanding of what and who is dysregulated in the disease context and ultimately give rise to potential new therapeutics targets.

The use of animal models has contributed for the purpose of understanding IPF pathogenesis [66,67,79]. One of the most accepted models is BLM-induced pulmonary fibrosis mouse model, which although presents some discrepancies, as fibrosis spontaneous resolution and lack of AECII hyperplasia, is the one with better reproducibility of pathological features of human disease [66,67]. Therefore, the importance of AEC II disfunction in the initial stage of pulmonary fibrosis was been demonstrated in several studies, which state that fibroproliferative processes can be initiated/perpetuated by poorly functioning AEC II [80]. Also, myofibroblasts are the known key effectors of fibrosis, with the increased capacity to produced exaggerated and disorganized ECM components [80–82]. However, recent progress in this field of investigation has been revealing the role of inflammation and more specifically of pulmonary MO, and their subpopulations in this organ. In this way, the work was focused on the roles of two main lung MO populations during the inflammatory phase of mouse lung fibrosis, more specifically the characterization of these populations during this phase, as well as understanding whether these macrophages regulate differentially fibroblasts transdifferentiation.

Lung macrophages populations, AMs and IMs, are highly heterogeneous cells as they have the capacity to adapt and respond to different anatomical locations, perform specialized functions within those sites and assume transient activation states [83,84]. Thus, they have the ability to promote or inhibit tissue remodeling during fibroproliferative contexts like pulmonary fibrosis [59,85].

There are few papers that identify and quantify the percentages of both MO populations and none of them analyzed these populations throughout the different time-points of inflammatory phase of BLM-induced pulmonary fibrosis. Thus, we took advantage of most complete gating strategy, used by Misharin et al. 2013 [64], that allowed the elimination of several immune populations in order to increase the reliability in the obtained MO population. Taking into account the previous information, we first quantified the

percentages of these cells in four time-points of inflammatory phase. Our findings revealed that AMs and IMs populations respond differently to BLM administration, with AMs dropping drastically and IM increase exponentially comparing with naïve state. Furthermore, AMs maintained low percentages, while IMs presented a significant progressively increase.

As the first line of immune defense in the alveoli, AMs pool is altered when contacting with molecules that enter the alveoli, leading to remodeling and or replacing of this population [86,87]. Thus, the direct contact with the administered BLM, which induces breaks in DNA, can lead to cellular necrosis and apoptosis [88–90] and thus explain the decrease of AMs population after drug administration. Misharin et al. 2013 also showed that AMs were decreased at day 5 after BLM administration [64]. Moreover, at day 7 and 9 we observed a partially recover of this population, regardless of still very low levels comparing with naive and treated IMs values. This recovering can be explained by the recruitment of circulating monocytes that, upon injury, can replenishing AMs population [50,91].

IMs population functions are less known than AMs due to the relatively recent discovery of this cell population [52] and the inherent difficulties in defining, obtaining and characterizing it [46,47,53]. The development of mechanical and enzymatic techniques to harvest pulmonary macrophages allowed improvement in IMs understanding [53]. We took advantage of these techniques and associated them with flow cytometry, using the same strategy to identify the populations of interest at all analyzed time-points. This allowed us to observe that as the inflammatory phase progresses, IMs population increases, and continuous to increase as the inflammatory phase start to decline (day 9). The increased percentage of IMs at day 5 after BLM administration was already observed in the work of Misharin et al. 2013 [64]. Regarding the alveoli compartment, IMs are found in same narrow interalveolar space as AEC, fibroblasts and other mesenchymal cells, which promotes the direct contact with these pulmonary connective-tissue components, as well as their secreted mediators [49,83]. Thus, the changes in this lung compartment as pulmonary fibrosis develops can potentiate the biological and/or pathological response of IMs and lead to the observed increase on this population. Furthermore, no differences were observed in vehicle and control groups, which indicates that the alterations observed in IMs percentages are due to BLM administration consequences.

The outcomes so far discussed indicate that in terms of percentages the two populations are very different. Then, we goaled to unveil whether this would be translated into differentially functionalities in disease progression. In this way, we started by analyzing their activation profile in respond to lung injury, in a broader approach by studying CD80, CD206 and MHCII expression.

We observed several changes in the evolution of treated AMs and IMs regarding the percentage of CD80, CD206 and MHCII expressing cells, when comparing to the respective vehicle and control groups. These similarities suggest, that the BLM administration is stimulating alteration in the percentage of cells expressing these molecules, as expected. We detected a distinct phenotype regarding CD80, CD206 and MCHII expressing cells in treated IMs compared to treated AMs. IMs presented a tendency to increase the expression of the mentioned markers that was significantly different at day 7 and 9 for CD80 and MHCII, and at day 5, 7 and 9 for CD206 expression.

CD206, also known as macrophage mannose receptor, is expressed on the surface of these cells where it is involved in pathogen recognition. Thus, act as pathogen recognition receptor by binding to glycoproteins and glycolipids found on the surface of pathogens. This is followed by antigen internalization and presentation T cells, continuing the process of inflammatory recruitment and response [92,93]. IMs have been shown to acquire a pro-fibrotic phenotype, characterized by elevated expression of CD206 [63,64], which we also observed in our results and could be indicating the increased capacity to promote inflammation and consequently fibrosis progression.

The progression of pulmonary fibrosis is thought to be associated with and imbalance Th2 inflammatory response [36]. Antigen-presenting cells (APCs), namely macrophages and dendritic cells, play an important role in regulating immune responses. APCs express MHCII molecules, which allows them to bind and present antigens to $CD4^+$ T cells [94]. Besides the MHCII, co-stimulatory molecules like CD80 are necessary to ensure the activation of these T cells [94]. AMs and IMs express MHCII and exhibit antigen presenting activity. However, several studies of other pulmonary diseases show that AMs present a reduced antigen presenting activity relatively to dendritic cells and interstitial macrophages [95–97]. Interestingly, in McCubbrey. et al 2018, a gene that encodes the beta chain of MHCII is upregulated in treated IMs, in comparison to treated AMs [77]. Taking all this in consideration, our findings indicate that treated IMs could be acting as important antigen presenting cells, thus promoting the dysregulated inflammation through the activation of imbalance immunes responses, and consequently fibrosis progression.

Numerous mediators have been implied in the pathogenesis and progression of lung fibrosis. However, in order to correctly assess their function, it has to be taking into consideration that, depending on the stage of the fibrotic process, the same pro-inflammatory or anti-inflammatory mediator can be promoting or inhibiting fibrosis. To further dissect the activation profile of lung MO population, we decided to study the expression of several pro-inflammatory genes as well as anti-inflammatory and tissue-repair associated genes, in the time-point referred as the peak of the inflammatory phase, day 7. Although no

significative statistically differences were observed, probably to the low number of biological replicates, is important to highlight the most undoubtedly tendencies.

In general way, our data show gene expression alterations in treated AMs and IMs animal groups, when compared to the respective control. This indicates that BLM administration is leading to changes in the transcript pool of both treated MO, since it is inducing disease. Moreover, these two populations are different among each other, which can indicate a different response to the disease. Treated IMs present higher gene expression of *Ccl2* and *Ccl9* and lower expression of *Ccl5* and *Ccl6*, when compared to treated AMs. Moreover, treated IMs also presented higher expression of *Arg1*, *Tgfbi*, *Ccl24*, *Fn1*, *Mmp12* and *Retlna* and a lower expression of *Chi3l3*. The increase of referred genes goes accordingly to was is shown in McCubbrey. et al 2018, in which all mentioned genes are significantly increase in treated IMs at 8 days after BLM administration, when comparted to treated AMs [77]. Also, several of these molecules are described in this work and others as having a role in potentiating the fibrotic progression of the disease.

Chemokine/cytokine network is capable of modulating the different phases of lung fibrosis pathogenesis [98]. These mediators are produced by several cell types in the lung, including macrophages, and are responsible for promoting the mobilization and trafficking of circulating monocytes, T-cells, natural killer cells, fibrocytes, among other cells to the sites of injury. Thus, they promote the inflammatory response and fibrosis progression [99,100]. In the work of McCubbrey. et al 2018[77] is described that *Ccl2* , *Ccl24* and Ccl9 are strongly upregulated in murine CD11b^{hi} macrophages, that were identified as interstitial macrophages [77]. Interestingly, in a study of radiation-induced fibrosis that used chimeric mice, the mice that had received bone marrow lacking CCR2 (Ccl2 receptor) presented decreased number of infiltrating and interstitial macrophages, that correlated with no pulmonary fibrosis after 22 weeks post radiation [101]. Once, we suggest that Ccl2, Ccl9 and Ccl24 can be participating in the recruitment of monocytes that will increase the treated IMs population, increasing the inflammatory response at day 7 after BLM administration. Moreover, Ccl5 and Ccl6 are known to be produce by endothelial cells and fibroblasts and have a role in promoting fibrosis progression [102–104]. However, how the diminution of these chemokine ligands specifically by MO influences pulmonary fibrosis is not described. In this way, it would be interesting to further explore their role in fibrosis through lung macrophages.

Arg1 is a precursor for the synthesis of proline, which is an important component of collagen. Thus, the supply of proline can be a crucial factor in the process of lung fibrosis. Arg1 have been already described as increase in lung macrophages during pulmonary fibrosis [50,105,106]. However, this increase is described only for AMs, once the majority of studies until recently only focused in the role of AMs in pulmonary

fibrosis. McCubbrey. et al 2018 already reported that the expression of Arg1 is significantly increased in treated IMs, at 8 day after BLM administration [77]. Thus, it is important to understand if IMs Arg1 production is influencing fibrosis. Our results indicate that this molecule is more expressed by treated IMs than AMs, which can indicate that is regulating the role of IMs in fibrosis progression.

Mmp are a family of zinc-binding endopeptidases that through their proteolytic activity are involved in normal and pathological ECM turnover [107]. Their dysregulated activity is implicated in fibrosis progression [107]. Their roles are more extensive that degrading ECM components, once they can release, cleave and activate a wide range of growth factors, cytokines, chemokines, altering the fibrotic capacity of the micro-environment that surrounds them [108]. Mmp12 is mainly produced by macrophages [109,110]. Kang et al. 2007 showed that Mmp-12 has an important role in Tgf-1β effector pathway activation, as they observed that Tgf-1β-stimulated and bleomycin-stimulated pulmonary fibrosis were ameliorated in Mmp-12-deficient animals [111]. Also, Mmp12 was implicated in the fibrotic response of a model of fibrosis using Fas, where mice treated with Fas-activating antibody have increased caspase-3 activation in alveolar wall cells and increased total lung collagen on day 21 after exposure [112]. In this study, a gene expression profiling showed activation profibrotic genes, namely significant upregulation of Mmp12 and also when targeted deletion of MMP-12 was done, mice were protected from Fas-induced pulmonary [112].

Overall, the results of transcript expression analysis suggest that treated IMs have increased several genes, when comparted to treated AMs, that can potentiate their action through the development of a pro-fibrotic niche. These results are preliminary once we used a reduced biological samples number (n=3) in one independent experiment. Thus, is necessary to repeat this experiment in order to validate that the tendencies presented are translated into definitive differences.

So far, we had observed higher percentages of treated IMs throughout the assessed time-points of the inflammatory phase. Moreover, IMs presented a tendency to a pro-fibrotic phenotype at the 7, which corresponds to the peak of inflammatory phase. We then focused on the paracrine abilities of lung MO populations and their capacity to modulate the fibroblast transdifferentiation into myofibroblasts at the peak (day 7) and late (day 9) periods of the inflammatory phase. For that, we used *in vitro* assays in which fibroblasts from a mouse lung cell line were stimulated with conditioned media of primary culture sorted AMs and IMs from treated animals, at day 7 and day 9 after BLM administration. After the stimulation, we assessed if the conditioned media was affecting cell apoptosis, proliferation, transdifferentiation and metabolic activity.

Regarding the 7 days conditioned media assays, we observed that cells stimulated with treated AMs- and IMs-derived conditioned media presented higher levels of cell confluency, when compared to the other

experimental conditions. Interestingly, in these two conditions, adherence cells present increased cytoplasm and spindle-shaped morphology, which are typical characteristics found in myofibroblasts.

Regarding the apoptosis analysis, only the treated AMs-derived conditioned media was inducing some degree of apoptosis. This could be justified by the significant high levels of cell confluency observed, combined with cells presenting increased cytoplasm, which could potentiate stress and programmed cell death.

The stimulation with treated AMs- and IMs- derived conditioned media induced a increase trend in cell proliferation. This increase showed a tendency to be higher in treated IMs-derived conditioned media. The analyses of cell proliferative state went in agreement with the interpretations made regarding cell confluency, hence the conditions with higher levels of proliferative cells are the ones that present higher well surface covered with cells. Furthermore, treated AMs and IMs conditioned media also induced a tendency to elevated metabolic activity, which is in accordance with the results examined above. Thus, cells that are in active proliferative state normality present higher metabolic activity [113,114]. Moreover, the cells stimulated with treated IMs-derived conditioned media were the ones where adherent cells present highest levels of αSma and Vim positive cells and lower levels of Vim positive cells. This suggests that treated IMs-derived conditioned media promotes fibroblasts transdifferentiation into myofibroblasts, since the higher number of cells express αSma. These results are also in accordance with the interpretations made regarding cell morphology once the majority of cells stimulated with treated IMs-derived conditioned media presented increased cytoplasm and spindle-shaped morphology, morphological features of myofibroblast [115]. Interestingly, despite treated AMs and IMs conditioned media promote similar responses regarding cell confluency, morphology, proliferation and metabolic activity, the IMs show a higher capacity of promoting transdifferentiation of fibroblasts into myofibroblasts. These results suggest that treated IMs have more capacity to promote transdifferentiation and thus potentiate fibrosis. However, to claim this with more certainty, all these findings need to be replicated in several independent experiments.

Regarding the 9 days conditioned media *in vitro* assays, we observed that the wells stimulated with untreated and treated AMs-derived conditioned media presented lower cell confluency, while treated IMs wells showed higher cell confluency, when compared to the all other conditions. Contrary to what was observed in the 7 days conditioned media assays, cells did not present increased cytoplasm and spindle-shaped morphology in any conditions. Moreover, the untreated and treated AMs-derived conditioned media stimulated wells exhibited significant cellular debris in suspension. Interestingly, these two conditions presented cells staining positive for annexin V, indicating that a portion of adherent cells was in apoptotic process.

Cells stimulated with untreated and treated AMs-derived conditioned media presented less cell confluency and also showed lower levels of proliferation and metabolic activity. Altogether, the data indicate that in these cells could be in stress, once it was verified increase cell death and increase cellular debris in suspension. Moreover, in untreated and treated AMs-derived conditioned media stimulated cells, the overall low percentages of αSma and Vim positive cells and Vim only positive cells could be explained by the observations made regarding cell confluency and morphology. Interestingly, the treated IMs-derived conditioned media condition presented the highest levels of cell confluency which was accompanied by high percentages of proliferative cells and increased levels of αSma and Vim positive cells. Nevertheless, this condition presented similar levels of Vim only positive cells, when compared to the percentages of αSma and Vim positive cells. This could indicate that 9 days treated IMs-derived conditioned media is inducing some degree of transdifferentiation but not completely, once myofibroblasts are observed upon stimulation but are also present similar levels of fibroblasts, identified as of Vim only positive cells. However, the results of both AMs conditions at 9th day lead us to suspect of a technical problem may have occurred. Thus, is fundamental to repeat these experiments.

In resume, the data of the work included in thesis allow a better understanding of pulmonary macrophages populations across the inflammatory phase of bleomycin-induced pulmonary fibrosis. IMs population from BLM treated mice present a progressively increase throughout the analyzed time-points. This was combined with increased expression of genes several genes that are associated with the development of a pro-fibrotic niche. Furthermore, treated IMs-derived conditioned media induce fibroblast transdiferentiation, at the time-point correspondent to the peak of inflammatory phase. Together, our findings indicate that IMs are the principal lung macrophage population promoting fibrosis progression in the inflammatory phase of the BLM-induced pulmonary fibrosis mouse model.

6. Conclusions and Future Perspectives

The findings of this thesis point out IM population as the key trigger of inflammatory phase of BLM-induced pulmonary fibrosis model. In order to validate these data is necessary to increase the number of independent experiments, either in the lung MOs characterization as in the *in vitro* approach to study the interaction between these cell populations and fibroblasts. Also, it would be interesting to expand the transcript analysis of associated pro-inflammatory and anti-inflammatory genes performed at day 7, the peak of inflammatory phase of disease model, to the day 9 and 14, the beginning and peak of the fibrotic phase. This would allow to understand if the populations are changing their transcripts profile and consequently their functional phenotype, in the time course of disease progression model.

MO populations are known to be present in the fibrotic phase of pulmonary fibrosis and we observed that in the switch between the inflammatory and fibrotic phase (day 9), IMs are present in the highest number and AMs are slowly recovering their population. Thus, it would be of relevance to investigate the roles of pulmonary MO across the fibrotic phase.

7. Bibliography

1. Kreuter, M. et al. Palliative care in interstitial lung disease: living well. Lancet Respir. Med. **5**, 968–980 (2017).

2. Antoniou, K. M. et al. Interstitial lung disease. Eur. Respir. Rev. **23**, 40–54 (2014).

3. Mikolasch, T. A., Garthwaite, H. S. & Porter, J. C. Update in diagnosis and management of interstitial lung disease. Clin. Med. (Northfield. Il). **17**, 146–153 (2017).

4. Martinez, F. J. et al. Idiopathic pulmonary fibrosis. Nat. Rev. Dis. Prim. **3**, 17074 (2017).

5. Raghu, G. et al. An Official ATS/ERS/JRS/ALAT Statement: Idiopathic Pulmonary Fibrosis: Evidence-based Guidelines for Diagnosis and Management. Am. J. Respir. Crit. Care Med. **183**, 788–824 (2011).

6. Olson, A. L., Gifford, A. H., Inase, N., Fernández Pérez, E. R. & Suda, T. The epidemiology of idiopathic pulmonary fibrosis and interstitial lung diseases at risk of a progressive-fibrosing phenotype. Eur. Respir. Rev. **27**, 180077 (2018).

7. Hutchinson, J., Fogarty, A., Hubbard, R. & McKeever, T. Global incidence and mortality of idiopathic pulmonary fibrosis: a systematic review. Eur. Respir. J. **46**, 795–806 (2015).

8. Vancheri, C., Failla, M., Crimi, N. & Raghu, G. Idiopathic pulmonary fibrosis: a disease with similarities and links to cancer biology. Eur. Respir. J. **35**, 496–504 (2010).

9. Noble, P. W., Barkauskas, C. E. & Jiang, D. Pulmonary fibrosis: patterns and perpetrators. J. Clin. Invest. **122**, 2756–2762 (2012).

10. Lederer, D. J. & Martinez, F. J. Idiopathic Pulmonary Fibrosis. N. Engl. J. Med. **378**, 1811–1823 (2018).

11. Raghu, G. et al. Diagnosis of Idiopathic Pulmonary Fibrosis. An Official ATS/ERS/JRS/ALAT Clinical Practice Guideline. Am. J. Respir. Crit. Care Med. **198**, e44–e68 (2018).

12. Lynch, D. A. et al. Diagnostic criteria for idiopathic pulmonary fibrosis: a Fleischner Society White Paper. Lancet Respir. Med. **6**, 138–153 (2018).

13. Scelfo, C., Caminati, A. & Harari, S. Recent advances in managing idiopathic pulmonary fibrosis. F1000Res. **6**, 2052 (2017).

14. Pleasants, R. & Tighe, R. M. Management of Idiopathic Pulmonary Fibrosis. Ann. Pharmacother. **53**, 1238–1248 (2019).

15. Raghu, G. et al. An Official ATS/ERS/JRS/ALAT Clinical Practice Guideline: Treatment of Idiopathic Pulmonary Fibrosis. An Update of the 2011 Clinical Practice Guideline. Am. J. Respir. Crit. Care Med. **192**, e3–e19 (2015).

16. Ahluwalia, N., Shea, B. S. & Tager, A. M. New Therapeutic Targets in Idiopathic Pulmonary Fibrosis. Aiming to Rein in Runaway Wound-Healing Responses. Am. J. Respir. Crit. Care Med. **190**, 867–878 (2014).

17. Richeldi, L. et al. Efficacy and Safety of Nintedanib in Idiopathic Pulmonary Fibrosis. N. Engl. J. Med. **370**, 2071–2082 (2014).

18. Wollin, L. et al. Mode of action of nintedanib in the treatment of idiopathic pulmonary fibrosis. Eur. Respir. J. **45**, 1434–1445 (2015).

19. Noble, P. W. et al. Pirfenidone in patients with idiopathic pulmonary fibrosis (CAPACITY): two randomised trials. Lancet. **377**, 1760–1769 (2011).

20. King, T. E. et al. A Phase 3 Trial of Pirfenidone in Patients with Idiopathic Pulmonary Fibrosis. N. Engl. J. Med. **370**, 2083–2092 (2014).

21. Wuyts, W. A. et al. The pathogenesis of pulmonary fibrosis: a moving target. Eur. Respir. J. **41**, 1207–1218 (2013).

22. Sgalla, G. et al. Idiopathic pulmonary fibrosis: pathogenesis and management. Respir. Res. **19**, 32 (2018).

23. Ryu, J. H. et al. Idiopathic Pulmonary Fibrosis: Evolving Concepts. Mayo Clin. Proc. **89**, 1130–1142 (2014).

24. Jones, M. G. et al. Three-dimensional characterization of fibroblast foci in idiopathic pulmonary fibrosis. JCI insight. **1**, e86375 (2016).

25. Harari, S. & Caminati, A. IPF: new insight on pathogenesis and treatment. Allergy. **65**, 537–553 (2010).

26. Richeldi, L., Collard, H. R. & Jones, M. G. Idiopathic pulmonary fibrosis. Lancet. **389**, 1941–1952 (2017).

27. Wang, Y. et al. Pulmonary alveolar type I cell population consists of two distinct subtypes that differ in cell fate. Proc. Natl. Acad. Sci. **115**, 2407–2412 (2018).

28. Nabhan, A. N., Brownfield, D. G., Harbury, P. B., Krasnow, M. A. & Desai, T. J. Single-cell Wnt signaling niches maintain stemness of alveolar type 2 cells. Science. **359**, 1118–1123 (2018).

29. Winters, N. I., Burman, A., Kropski, J. A. & Blackwell, T. S. Epithelial Injury and Dysfunction in the Pathogenesis of Idiopathic PulmonaryFibrosis. Am. J. Med. Sci. **357**, 374–378 (2019).

30. Liang, J. et al. Hyaluronan and TLR4 promote surfactant-protein-C-positive alveolar progenitor cell renewal and prevent severe pulmonary fibrosis in mice. Nat. Med. **22**, 1285–1293 (2016).

31. Katzenstein, A. a & Myers, J. L. Idiopathic Pulmonary Fibrosis Clinical Relevance of Pathologic Classification Clinical Features of the Idiopathic Interstitial Pneumonias. Am. J. Respir. Crit. Care Med. **157**, 1301-1315 (1998).

32. Korfei, M. et al. Epithelial Endoplasmic Reticulum Stress and Apoptosis in Sporadic Idiopathic Pulmonary Fibrosis. Am. J. Respir. Crit. Care Med. **178**, 838–846 (2008).

33. Kolahian, S., Fernandez, I. E., Eickelberg, O. & Hartl, D. Immune Mechanisms in Pulmonary Fibrosis. Am. J. Respir. Cell Mol. Biol. **55**, 309–322 (2016).

34. Selman, M., López-Otín, C. & Pardo, A. Age-driven developmental drift in the pathogenesis of idiopathic pulmonary fibrosis. Eur. Respir. J. **48**, 538–552 (2016).

35. Walsh, S. M. et al. Novel differences in gene expression and functional capabilities of myofibroblast populations in idiopathic pulmonary fibrosis. Am. J. Physiol. Cell. Mol. Physiol. **315**, L697–L710 (2018).

36. Ballester, B., Milara, J. & Cortijo, J. Idiopathic Pulmonary Fibrosis and Lung Cancer: Mechanisms and Molecular Targets. Int. J. Mol. Sci. **20**, 593 (2019).

37. Coward, W. R., Saini, G. & Jenkins, G. The pathogenesis of idiopathic pulmonary fibrosis. Ther. Adv. Respir. Dis. **4**, 367–388 (2010).

38. Hinz, B. Mechanical Aspects of Lung Fibrosis. Proc. Am. Thorac. Soc. **9**, 137–147 (2012).

39. Barron, L., Gharib, S. A. & Duffield, J. S. Lung Pericytes and Resident Fibroblasts. Am. J. Pathol. **186**, 2519–2531 (2016).

40. Heukels, P. et al. Fibrocytes are increased in lung and peripheral blood of patients with idiopathic pulmonary fibrosis. Respir. Res. **19**, 90 (2018).

41. Maharaj, S., Shimbori, C. & Kolb, M. Fibrocytes in pulmonary fibrosis: a brief synopsis. Eur. Respir. Rev. **22**, 552–557 (2013).

42. Andersson-Sjöland, A. et al. Fibrocytes are a potential source of lung fibroblasts in idiopathic pulmonary fibrosis. Int. J. Biochem. Cell Biol. **40**, 2129–2140 (2008).

43. Salton, F., Volpe, M. C. & Confalonieri, M. Epithelial–Mesenchymal Transition in the Pathogenesis of Idiopathic Pulmonary Fibrosis. Medicina. **55**, 83 (2019).

44. Wynn, T. A. Integrating mechanisms of pulmonary fibrosis. J. Exp. Med. **208**, 1339–1350 (2011).

45. Heukels, P., Moor, C. C., von der Thüsen, J. H., Wijsenbeek, M. S. & Kool, M. Inflammation and immunity in IPF pathogenesis and treatment. Respir. Med. **147**, 79–91 (2019).

46. Liegeois, M., Legrand, C., Desmet, C. J., Marichal, T. & Bureau, F. The interstitial macrophage: A long-neglected piece in the puzzle of lung immunity. Cell. Immunol. **330**, 91–96 (2018).

47. Gibbings, S. L. et al. Three Unique Interstitial Macrophages in the Murine Lung at Steady State. Am. J. Respir. Cell Mol. Biol. **57**, 66–76 (2017).

48. Zhou, X. & Moore, B. B. Location or origin? What is critical for macrophage propagation of lung fibrosis? Eur. Respir. J. **51**, 1800103 (2018).

49. Tan, S. Y. S. & Krasnow, M. A. Developmental origin of lung macrophage diversity. Development **143**, 1318–27 (2016).

50. Misharin, A. V. et al. Monocyte-derived alveolar macrophages drive lung fibrosis and persist in the lung over the life span. J. Exp. Med. **214**, 2387–2404 (2017).

51. Byrne, A. J., Mathie, S. A., Gregory, L. G. & Lloyd, C. M. Pulmonary macrophages: key players in the innate defence of the airways. Thorax. **70**, 1189–1196 (2015).

52. Koch, C. M., Chiu, S. F., Misharin, A. V & Ridge, K. M. Lung Interstitial Macrophages: Establishing Identity and Uncovering Heterogeneity. Am. J. Respir. Cell Mol. Biol. **57**, 7–9 (2017).

53. Schyns, J., Bureau, F. & Marichal, T. Lung Interstitial Macrophages: Past, Present, and Future. J. Immunol. Res. **2018**, 5160794 (2018).

54. Duffield, J. S. et al. Selective depletion of macrophages reveals distinct, opposing roles during liver injury and repair. J. Clin. Invest. **115**, 56–65 (2005).

55. Desai, O., Winkler, J., Minasyan, M. & Herzog, E. L. The Role of Immune and Inflammatory Cells in Idiopathic Pulmonary Fibrosis. Front. Med. **5**, 43 (2018).

56. Zhang, L. et al. Macrophages: friend or foe in idiopathic pulmonary fibrosis? Respir. Res. **19**, 170 (2018).

57. Song, E. et al. Influence of Alternatively and Classically Activated Macrophages on Fibrogenic Activities of Human Fibroblasts. Cell. Immunol. **204**, 19–28 (2000).

58. Wynn, T. & Barron, L. Macrophages: Master Regulators of Inflammation and Fibrosis. Semin. Liver Dis. **30**, 245–257 (2010).

59. Byrne, A. J., Maher, T. M. & Lloyd, C. M. Pulmonary Macrophages: A New Therapeutic Pathway in Fibrosing Lung Disease? Trends Mol. Med. **22**, 303–316 (2016).

60. Morse, C. et al. Proliferating SPP1/MERTK-expressing macrophages in idiopathic pulmonary fibrosis. Eur. Respir. J. **54**, 1802441 (2019).

61. Reyfman, P. A. et al. Single-Cell Transcriptomic Analysis of Human Lung Provides Insights into the Pathobiology of Pulmonary Fibrosis. Am. J. Respir. Crit. Care Med. **199**, 1517–1536 (2019).

62. Pechkovsky, D. V et al. Alternatively activated alveolar macrophages in pulmonary fibrosis–mediator production and intracellular signal transduction. Clin. Immunol. **137**, 89–101 (2010).

63. Ji, W.-J. et al. Temporal and spatial characterization of mononuclear phagocytes in circulating, lung alveolar and interstitial compartments in a mouse model of bleomycin-induced pulmonary injury. J. Immunol. Methods. **403**, 7–16 (2014).

64. Misharin, A. V, Morales-Nebreda, L., Mutlu, G. M., Budinger, G. R. S. & Perlman, H. Flow Cytometric Analysis of Macrophages and Dendritic Cell Subsets in the Mouse Lung. Am. J. Respir. Cell Mol. Biol. **49**, 503–510 (2013).

65. Meziani, L. et al. CSF1R inhibition prevents radiation pulmonary fibrosis by depletion of interstitial macrophages. Eur. Respir. J. **51**, 1702120 (2018).

66. O'Dwyer, D. N. & Moore, B. B. Animal Models of Pulmonary Fibrosis.Methods Mol. Biol. **1809**, 363–378 (2018).

67. Tashiro, J. et al. Exploring Animal Models That Resemble Idiopathic Pulmonary Fibrosis. Front. Med. **4**, 118 (2017).

68. Liu, T., De Los Santos, F. G. & Phan, S. H. The Bleomycin Model of Pulmonary Fibrosis. Methods. Mol. Biol. **1627**, 27–42 (2017).

69. Wei, Y.-R. et al. Establishment of the mouse model of acute exacerbation of idiopathic pulmonary fibrosis. Exp. Lung Res. **42**, 75–86 (2016).

70. Kim, S.-N. et al. Dose-response Effects of Bleomycin on Inflammation and Pulmonary Fibrosis in Mice. Toxicol. Res. **26**, 217–222 (2010).

71. Moeller, A., Ask, K., Warburton, D., Gauldie, J. & Kolb, M. The bleomycin animal model: A useful tool to investigate treatment options for idiopathic pulmonary fibrosis? Int. J. Biochem. Cell Biol. **40**, 362–382 (2008).

72. Mouratis, M. A. & Aidinis, V. Modeling pulmonary fibrosis with bleomycin. Curr. Opin. Pulm. Med. **17**, 355–361 (2011).

73. Lawson, W. E. et al. Increased and Prolonged Pulmonary Fibrosis in Surfactant Protein C-Deficient Mice Following Intratracheal Bleomycin. Am. J. Pathol. **167**, 1267–1277 (2005).

74. Livak, K. J. & Schmittgen, T. D. Analysis of Relative Gene Expression Data Using Real-Time Quantitative PCR and the 2−ΔΔCT Method. Methods. **25**, 402–408 (2001).

75. Yamasaki, K. & Eeden, S. F. van. Lung Macrophage Phenotypes and Functional Responses: Role in the Pathogenesis of COPD. Int. J. Mol. Sci. **19**, 582 (2018).

76. Novak, M. L. & Koh, T. J. Macrophage phenotypes during tissue repair. J. Leukoc. Biol. **93**, 875–881 (2013).

77. McCubbrey, A. L. et al. Deletion of c-FLIP from CD11bhi Macrophages Prevents Development of Bleomycin-induced Lung Fibrosis. Am. J. Respir. Cell Mol. Biol. **58**, 66–78 (2018).

78. Kropski, J. A. & Blackwell, T. S. Progress in Understanding and Treating Idiopathic Pulmonary Fibrosis. Annu. Rev. Med. **70**, 211–224 (2019).

79. Moeller, A., Rodriguez-Lecompte, J. C., Wang, L., Gauldie, J. & Kolb, M. Models of pulmonary fibrosis. Drug Discov. Today Dis. Model. **3**, 243–249 (2006).

80. Wolters, P. J., Collard, H. R. & Jones, K. D. Pathogenesis of Idiopathic Pulmonary Fibrosis. Annu. Rev. Pathol. Mech. Dis. **9**, 157–179 (2014).

81. Black, M. et al. FOXF1 Inhibits Pulmonary Fibrosis by Preventing CDH2-CDH11 Cadherin Switch in Myofibroblasts. Cell Rep. **23**, 442–458 (2018).

82. Darby, I. A., Zakuan, N., Billet, F. & Desmoulière, A. The myofibroblast, a key cell in normal and pathological tissue repair. Cell. Mol. Life Sci. **73**, 1145–1157 (2016).

83. Laskin, D. L., Weinberger, B. & Laskin, J. D. Functional heterogeneity in liver and lung macrophages. J. Leukoc. Biol. **70**, 163–170 (2001).

84. Schneberger, D., Aharonson-Raz, K. & Singh, B. Monocyte and macrophage heterogeneity and Toll-like receptors in the lung. Cell and Tissue Research **343**, 97–106 (2011).

85. Borthwick, L. A., Wynn, T. A. & Fisher, A. J. Cytokine mediated tissue fibrosis. Biochim. Biophys. Acta. **1832**, 1049–60 (2013).

86. Morales-Nebreda, L., Misharin, A. V, Perlman, H. & Budinger, G. R. S. The heterogeneity of lung macrophages in the susceptibility to disease. Eur. Respir. Rev. **24**, 505–509 (2015).

87. Westphalen, K. et al. Sessile alveolar macrophages communicate with alveolar epithelium to modulate immunity. Nature. **506**, 503–506 (2014).

88. Ortiz, L. A. et al. Alveolar macrophage apoptosis and TNF-alpha, but not p53, expression correlate with murine response to bleomycin. Am. J. Physiol. **275**, L1208-18 (1998).

89. Chen, J., Ghorai, M. K., Kenney, G. & Stubbe, J. A. Mechanistic studies on bleomycin-mediated DNA damage: Multiple binding modes can result in double-stranded DNA cleavage. Nucleic Acids Res. **36**, 3781–3790 (2008).

90. Zhao, H. W. et al. Time-dependent apoptosis of alveolar macrophages from rats exposed to bleomycin: involvement of tnf receptor 2. J. Toxicol. Environ. Heal. **67**, 1391–1406 (2004).

91. Vlahos, R. & Bozinovski, S. Role of Alveolar Macrophages in Chronic Obstructive Pulmonary Disease. Front. Immunol. **5**, 435 (2014).

92. Martinez-Pomares, L. The mannose receptor. J. Leukoc. Biol. **92**, 1177–1186 (2012).

93. Azad, A. K., Rajaram, M. V. S. & Schlesinger, L. S. Exploitation of the Macrophage Mannose Receptor (CD206) in Infectious Disease Diagnostics and Therapeutics. J. Cytol. Mol. Biol. **1**, 1000003 (2014).

94. Chen, L. & Flies, D. B. Molecular mechanisms of T cell co-stimulation and co-inhibition. Nat. Rev. Immunol. **13**, 227–42 (2013).

95. Lohmann-Matthes, M. L., Steinmüller, C. & Franke-Ullmann, G. Pulmonary macrophages. Eur. Respir. J. **7**, 1678–89 (1994).

96. Steinmüller, C., Franke-Ullmann, G., Lohmann-Matthes, M.-L. & Emmendörffer, A. Local Activation of Nonspecific Defense against a Respiratory Model Infection by Application of Interferon- γ. Am. J. Respir. Cell Mol. Biol. **22**, 481–490 (2000).

97. Bedoret, D. et al. Lung interstitial macrophages alter dendritic cell functions to prevent airway allergy in mice. J. Clin. Invest. **119**, 3723–38 (2009).

98. Agostini, C. & Gurrieri, C. Chemokine/cytokine cocktail in idiopathic pulmonary fibrosis. Proc. Am. Thorac. Soc. **3**, 357–63 (2006).

99. Strieter, R. M., Gomperts, B. N. & Keane, M. P. The role of CXC chemokines in pulmonary fibrosis. J. Clin. Invest. **117**, 549–556 (2007).

100. Sahin, H. & Wasmuth, H. E. Chemokines in tissue fibrosis. Biochim. Biophys. Acta - Mol. Basis Dis. **1832**, 1041–1048 (2013).

101. Groves, A. M., Johnston, C. J., Williams, J. P. & Finkelstein, J. N. Role of Infiltrating Monocytes in the Development of Radiation-Induced Pulmonary Fibrosis. Radiat. Res. **189**, 300–311 (2018).

102. Berres, M.-L. et al. Antagonism of the chemokine Ccl5 ameliorates experimental liver fibrosis in mice. J. Clin. Invest. **120**, 4129–4140 (2010).

103. Pierce, E. M. et al. Idiopathic pulmonary fibrosis fibroblasts migrate and proliferate to CC chemokine ligand 21. Eur. Respir. J. **29**, 1082–1093 (2007).

104. Leach, H. G., Chrobak, I., Han, R. & Trojanowska, M. Endothelial Cells Recruit Macrophages and Contribute to a Fibrotic Milieu in Bleomycin Lung Injury. Am. J. Respir. Cell Mol. Biol. **49**, 1093–1101 (2013).

105. Endo, M. et al. Induction of arginase I and II in bleomycin-induced fibrosis of mouse lung. Am. J. Physiol. Cell. Mol. Physiol. **285**, L313–L321 (2003).

106. Kitowska, K. et al. Functional role and species-specific contribution of arginases in pulmonary fibrosis. Am. J. Physiol. Cell. Mol. Physiol. **294**, L34–L45 (2008).

107. Dancer, R. C. A., Wood, A. M. & Thickett, D. R. Metalloproteinases in idiopathic pulmonary fibrosis. Eur. Respir. J. **38**, 1461–1467 (2011).

108. Pardo, A., Cabrera, S., Maldonado, M. & Selman, M. Role of matrix metalloproteinases in the pathogenesis of idiopathic pulmonary fibrosis. Respir. Res. **17**, 23 (2016).

109. Madala, S. K. et al. Matrix Metalloproteinase 12-Deficiency Augments Extracellular Matrix Degrading Metalloproteinases and Attenuates IL-13–Dependent Fibrosis. J. Immunol. **184**, 3955–3963 (2010).

110. Aristorena, M. et al. MMP-12, Secreted by Pro-Inflammatory Macrophages, Targets Endoglin in Human Macrophages and Endothelial Cells. Int. J. Mol. Sci. **20**, 3107 (2019).

111. Kang, H.-R., Cho, S. J., Lee, C. G., Homer, R. J. & Elias, J. A. Transforming Growth Factor (TGF)-β 1 Stimulates Pulmonary Fibrosis and Inflammation via a Bax-dependent, Bid-activated Pathway That Involves Matrix Metalloproteinase-12. J. Biol. Chem. **282**, 7723–7732 (2007).

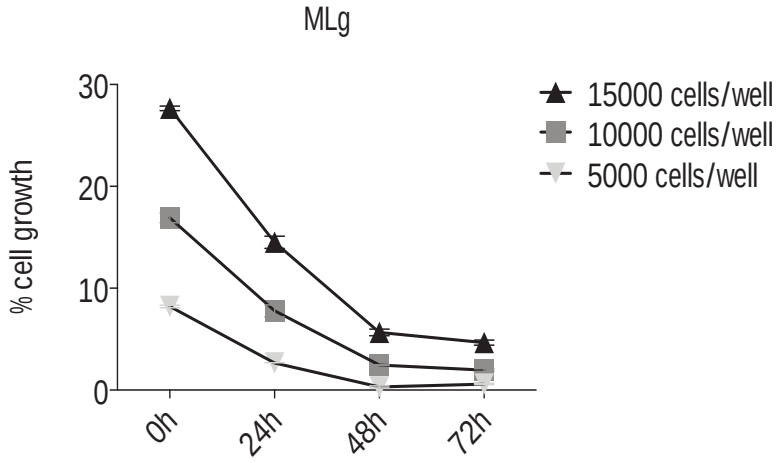
112. Matute-Bello, G. et al. Essential Role of MMP-12 in Fas-Induced Lung Fibrosis. Am. J. Respir. Cell Mol. Biol. **37**, 210–221 (2007).

113. DeBerardinis, R. J., Lum, J. J., Hatzivassiliou, G. & Thompson, C. B. The Biology of Cancer: Metabolic Reprogramming Fuels Cell Growth and Proliferation. Cell Metab. **7**, 11–20 (2008).

114. Zhu, J. & Thompson, C. B. Metabolic regulation of cell growth and proliferation. Nat. Rev. Mol. Cell Biol. **20**, 436–450 (2019).

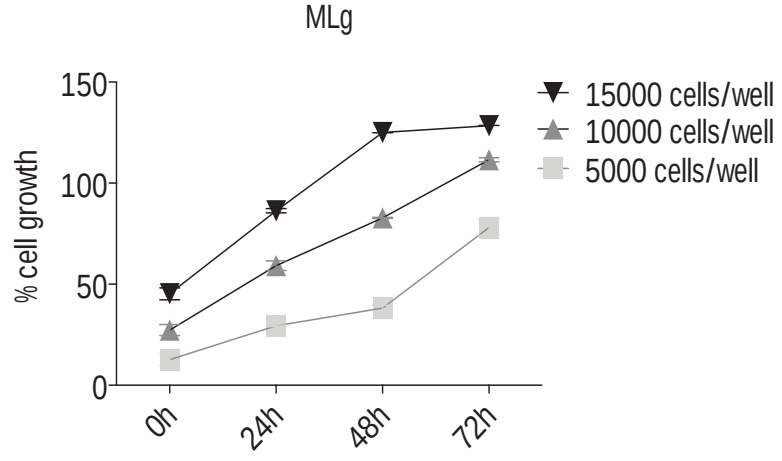
115. Phan, S. H. Biology of Fibroblasts and Myofibroblasts. Proc. Am. Thorac. Soc. **5**, 334–337 (2008).

8. Annexes



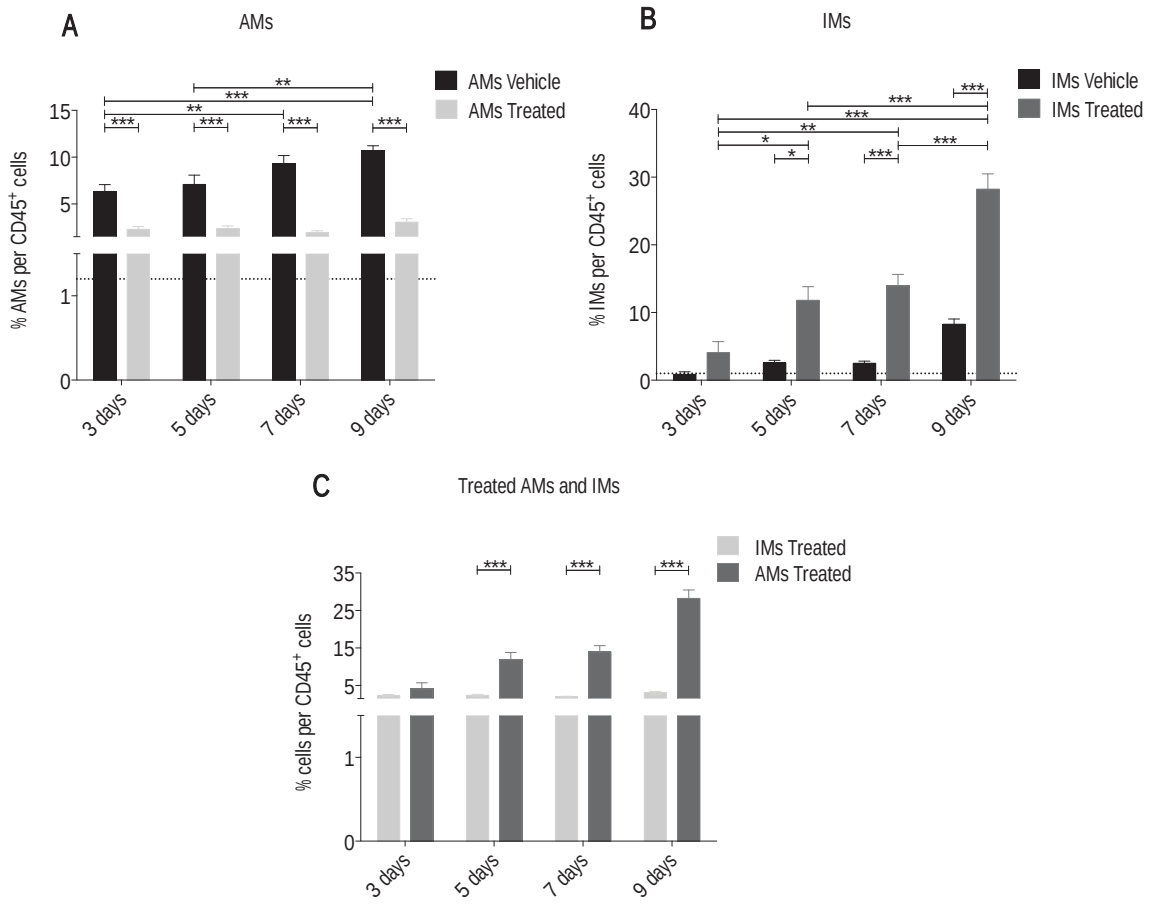
Supplementary Figure 1 - MLg cell line is not able to growth in culture without media supplementation with FBS.

Three different concentrations of MLg cells were plated in their culture media where let to adhere overnight. After this period, media was removed, cells washed with PBS1x, DMEM1x was added to the wells and cells were cultured for 24 h or 48 h. In order to assess the evolution of cell mass over-time, SRB assay was performed after the adherence period and after 24 and 48 h of culture. Data presented as mean±SEM. Each experiment was performed in triplicated and in 3 independent experiments.



Supplementary Figure 2 - Cell seeding density selection for in-vitro assays.

Three different concentrations of MLg cells were plated in their culture media where let to adhere overnight. After this period, media was removed, cells washed with PBS1x, DMEM1x/10%FBS was added to the wells and cells were cultured for 24 h or 48 h. In order to assess the evolution of cell mass over-time, SRB assay was performed after the adherence period and after 24 and 48 h of culture. The cell seeding density selection was based on the condition where the cells did not reach 100% cell growth, does having area to growth and proliferate whether necessary. Data presented as mean±SEM. Each experiment was performed in triplicated and in 3 independent experiments.



Supplementary Figure 3 - Characterization of macrophage population, AMs and IMs, dynamics at four time-points (3, 5, 7 9 days after BLM administration) of the inflammatory phase of pulmonary fibrosis using the gating strategy applied for the fluorescence activated cell sorting.

MO cytometry analysis was performed using the gating strategy applied for the fluorescence activated cell sorting, presented in figure 7. The percentages of lung MO populations obtained were similar to the ones obtained by the more complete gating strategy presented in figure 6.

AMs (A) were identified as $CD45^{+}CD11b^{+/-}CD11c^{+}CD64^{+}$ $Sigle\text{-}F^{+}$ and IMs (B) as $CD45^{+}CD11b^{+/-}CD11c^{+/-}CD64^{+}Sigle\text{-}F^{-}$ by flow cytometry within the $CD45^{+}$ population. MO cytometry analysis was performed in untreated (baseline), vehicle and treated groups. Percentages of treated AMs vs treated IMs are represented in (C). Data presented as mean±SEM (* $p < 0.05$; ** $p < 0.01$; *** $p < 0.001$).